

# Hold me tight! Influence of discriminative features on deep network boundaries

Guillermo Ortiz-Jiménez<sup>\*1</sup> Apostolos Modas<sup>\*1</sup> Seyed-Mohsen Moosavi-Dezfooli<sup>2</sup> Pascal Frossard<sup>1</sup>

## Abstract

Important insights towards the explainability of neural networks and their properties reside in the formation of their decision boundaries. In this work, we borrow tools from the field of adversarial robustness and propose a new framework that permits to relate the features of the dataset with the distance of data samples to the decision boundary along specific directions. We demonstrate that the inductive bias of deep learning has the tendency to generate classification functions that are invariant along non-discriminative directions of the dataset. More surprisingly, we further show that training on small perturbations of the data samples are sufficient to completely change the decision boundary. This is actually the characteristic exploited by the so-called adversarial training to produce robust classifiers. Our general framework can be used to reveal the effect of specific dataset features on the macroscopic properties of deep models and to develop a better understanding of the successes and limitations of deep learning.

## 1. Introduction

The set of points that partitions the input space onto labeled regions is known as the *decision boundary* of a classifier. Understanding how a classifier fits the training data and creates such boundaries is crucial for interpretability. For neural networks, the main properties of the decision boundary have been studied in the literature (Fawzi et al., 2018; He et al., 2018; Ramamurthy et al., 2019), mainly from a robustness point of view. Interestingly, even when deep networks perform very well on a task, their extreme vulnerability to adversarial perturbations (Szegedy et al., 2014; Goodfellow et al., 2015) implies that their boundaries still lie alarmingly close to any input sample. It has recently

<sup>\*</sup>Equal contribution <sup>1</sup>Ecole Polytechnique Fédérale de Lausanne (EPFL), Switzerland <sup>2</sup>Eidgenössische Technische Hochschule Zürich (ETHZ), Switzerland. Correspondence to: Guillermo Ortiz-Jiménez <guillermo.ortizjimenez@epfl.ch>, Apostolos Modas <apostolos.modas@epfl.ch>.

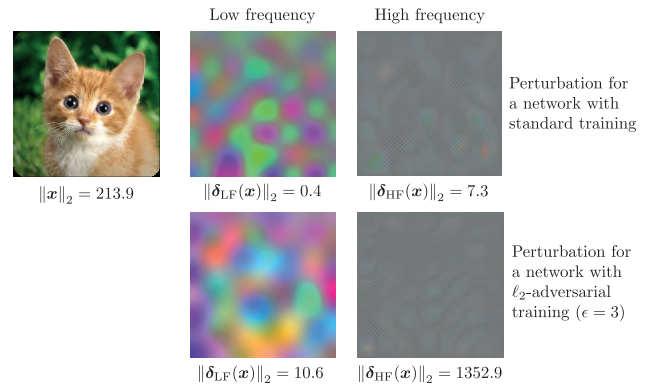


Figure 1. Minimal adversarial perturbations constrained to lie in different DCT frequency bands ( $8 \times 8$  subspaces taken from the top left and bottom right of the  $224 \times 224$  DCT matrix) for a ResNet-50 trained (**top**), and adversarially trained (**bottom**) on ImageNet. The numbers below the images show the  $\ell_2$ -norm of the perturbations.

been conjectured that adversarial examples are not a bug of the learning process, but a consequence of the abundance of brittle features in the datasets (Jetley et al., 2018; Ilyas et al., 2019). Considering this, it is natural to ask: How do neural networks actually construct their decision boundaries? And, can we really identify which features of the data they exploit?

Figure 1 provides an illustrative example of some of the intriguing properties that could be explained by studying the construction of decision boundaries. It shows the minimal perturbations – constrained to lie on a low and a high frequency subspace of the same dimensionality, respectively – required to flip the decision of a state-of-the-art deep network. The magnitude of these perturbations measures the distance to the decision boundary (margin) within these subspaces, and it is clear that much more energy is required to reach the boundary using high frequency perturbations, compared to low frequency ones (Sharma et al., 2019). Besides, it has been shown that it is much easier to train a network using only low frequency features, compared to high frequency ones (Yin et al., 2019). So, is it possible that the margin values across the spectrum are connected to how the discriminative features are distributed inside it?

These margin values are even more puzzling when we focus on the dramatic increase in margin along high frequencies when the network is trained using  $\ell_2$ -adversarial examples (Madry et al., 2018). Especially considering that the standard network was already robust in the high frequencies – i.e., the margin in this subspace was much higher than the norm of the training perturbations –, and hence one would expect that the largest increase in margin would be along the, more vulnerable, low frequency spectrum.

These surprising effects of the training dynamics can be more generally summarized in the following questions:

1. *How is the margin in different directions related to the training features?*
2. *How does the learning algorithm use the training samples to shape the decision boundaries?*

We contribute to answering these questions by proposing a new perspective that connects the microscopic features of the dataset (i.e., position of the training samples in the input space) to macroscopic properties of the learned models (e.g., margin distribution). Our main contributions are the following:

- We define a new experimental framework that allows to build a local summary of the decision boundaries of state-of-the-art classifiers from margin observations along a sequence of orthogonal directions. This enables us to carefully tweak the properties of the training samples and measure the induced changes on the boundaries of the networks.
- Using this setup, we demonstrate the existence of an inductive bias in neural networks towards invariance along non-discriminative directions.
- We show that in computer vision tasks, deep neural networks tend to exploit mainly discriminative features present in the low frequencies and ignore the information contained in the high frequencies.
- In general, the construction of the decision boundary is extremely sensitive to the position of the training samples. Small changes in their location can yield classifiers with very different geometric properties. In particular, we demonstrate that the so-called adversarial training exploits the invariance bias and sensitivity of the training algorithm to produce more robust classifiers.

We believe that the perspective proposed in this paper can have potential implications in future research on interpretability and robustness, and it can shed light onto the type of inductive bias that might explain the successes of deep learning, but also some of its limitations.

## 2. Related work

Since the publication of (Zhang et al., 2017), a big body of research has focused on understanding the implicit and inductive bias of deep networks as a way to explain generalization in deep learning (Gunasekar et al., 2018; Belkin et al., 2019). Remarkably, it has recently been proved that for linear classifiers, optimizing a logistic loss using gradient descent is equivalent to maximizing margin in the input space (Soudry et al., 2018). Nevertheless, it remains unclear whether these results can be translated to explain the decision boundary construction of deep non-linear models. Some new connections between SVMs and neural networks have recently been published (Li et al., 2018), although focused on the margin maximization properties of deep networks on the logit, rather than in the input space.

Another body of work has focused on analysing the geometric properties of the decision boundaries of deep networks, and showed that they are curved only along a small set of directions (Fawzi et al., 2018; Moosavi-Dezfooli et al., 2019), and that their enclosing decision regions are mostly connected when trained on natural high-dimensional datasets (Fawzi et al., 2018; Ramamurthy et al., 2019). From a robustness perspective, other authors have analyzed the distance to the boundary along random directions, claiming that its distribution can be exploited to detect adversarial examples (He et al., 2018). Previous authors have specifically studied the robustness of deep networks in different spatial frequencies, both to random colored noise (Yin et al., 2019), and to constrained adversarial examples crafted to a particular frequency band (Tsuzuku & Sato, 2019; Sharma et al., 2019). However, these works do not address the underlying causes that explain the differences in robustness in the Fourier domain. Recent studies have also shown that the distribution of approximate minimum distances to the boundary can be predictive of the generalization gap on a network (Elsayed et al., 2018; Jiang et al., 2019).

Interestingly, recent works have established the link between adversarial perturbations and discriminative features of the training sets (Jetley et al., 2018; Ilyas et al., 2019; Santurkar et al., 2019). This has led to the conjecture that in most datasets there exist robust and non-robust features that neural networks exploit to construct their decision boundaries. What exactly are these features, and how do networks construct these boundaries is however not addressed by these authors. We exactly try to bridge this gap in our work.

## 3. Proposed framework

Let  $f : \mathbb{R}^D \rightarrow \mathbb{R}^L$  be the final layer of a neural network (i.e., logits), such that, for any input  $\mathbf{x} \in \mathbb{R}^D$ ,  $F(\mathbf{x}) = \operatorname{argmax}_k f_k(\mathbf{x})$  represents the decision function of that network, where  $f_k(\mathbf{x})$  denotes the  $k$ ’th component of

$f(\mathbf{x})$  that corresponds to the  $k$ th class. The decision boundary between classes  $k$  and  $\ell$  of a neural network is the set of points  $\mathcal{B}_{k,\ell}(f) = \{\mathbf{x} \in \mathbb{R}^D : f_k(\mathbf{x}) - f_\ell(\mathbf{x}) = 0\}$  (in general, we will omit the dependency with  $k, \ell$  for simplicity). Unless stated otherwise, we assume that all networks are trained using a cross-entropy loss function and some variant of (stochastic) gradient descent (SGD). We also assume that training has been conducted for many epochs, and that it has approximately converged to a local minimum of the loss, achieving 100% accuracy on the training data (Zhang et al., 2017).

In this work, we study the role that the training set  $\mathcal{T} = \{(\mathbf{x}^{(i)}, y^{(i)})\}_{i=0}^{N-1}$  has on the construction of  $\mathcal{B}(f)$ . Specifically, we propose to use adversarial proxies to measure the distribution of distances to the decision boundary along a sequence of well defined subspaces. In this sense, the main quantities of interest are:

**Definition 1** (Minimal adversarial perturbations). *Given a classifier  $F$ , a sample  $\mathbf{x} \in \mathbb{R}^D$ , and a sub-region of the input space  $\mathcal{S} \subseteq \mathbb{R}^D$ , we define the ( $\ell_2$ ) minimal adversarial perturbation of  $\mathbf{x}$  in  $\mathcal{S}$  as*

$$\delta_{\mathcal{S}}(\mathbf{x}) = \operatorname{argmin}_{\delta \in \mathcal{S}} \|\delta\|_2 \quad \text{s.t.} \quad F(\mathbf{x} + \delta) \neq F(\mathbf{x}).$$

In general, whenever  $\mathbf{u} \in \mathbb{S}^{D-1}$  denotes a unit-norm vector in  $\mathbb{R}^D$  (direction) we will use  $\delta_{\mathbf{u}}(\mathbf{x})$  meaning  $\delta_{\operatorname{span}\{\mathbf{u}\}}(\mathbf{x})$ . Similarly, we will use  $\delta(\mathbf{x})$  to refer to  $\delta_{\mathbb{R}^D}(\mathbf{x})$ .

**Definition 2** (Margin). *The magnitude  $\|\delta_{\mathcal{S}}(\mathbf{x})\|_2$  is the margin of  $\mathbf{x}$  in  $\mathcal{S}$ .*

The main objective of our experimental setting is to obtain a local summary of  $\mathcal{B}(f)$  around a set of observation samples  $\mathcal{O} = \{\mathbf{x}^{(i)}\}_{i=0}^{M-1}$  by measuring their margin in a sequence of distinct subspaces  $\{\mathcal{S}_j\}_{j=0}^{R-1}$ . In practice, we use a subspace-constrained version of DeepFool (Moosavi-Dezfooli et al., 2016)<sup>1</sup> to approximate the margin of each  $\mathbf{x}^{(i)}$  in the directions specified by  $\mathcal{S}_j$ <sup>2</sup>.

All training and evaluation setups, including hyperparameters, number of observation samples, subspace parameters, and network performances are listed in the Supp. material.

## 4. Invariance and discriminative features

As known from previous studies on the robustness of deep learning (Fawzi et al., 2017), the distance from a sample to the boundary of a neural network can vary greatly depending on the search direction. In this work, we show that the implicit bias of the training dynamics pushes the networks

<sup>1</sup>We do not enforce the  $[0, 1]^D$  box constraints on the adversarial images, as we are not interested in finding ‘‘plausible’’ adversarial perturbations, but in measuring the distance to  $\mathcal{B}(f)$ .

<sup>2</sup>If the application requires it, the approximation is refined using backtracking binary search on the direction of DeepFool.

Table 1. Margin statistics of an MLP trained on  $\mathcal{T}_1(\epsilon = 5, \sigma = 1, N = 10,000)$  along different directions ( $M = 1,000, S = 3$ ).

	$\mathbf{u}_1$	$\operatorname{span}\{\mathbf{u}_1\}^\perp$	$\mathcal{S}_{\text{ORTH}}$	$\mathcal{S}_{\text{RAND}}$
5-PERCENT.	1.74	4.85	30.68	17.21
MEDIAN	2.50	12.36	102.0	27.90
95-PERCENT.	3.22	31.60	229.5	80.61

to become invariant along non-discriminative directions and construct boundaries only along discriminative ones. Therefore, since in most networks the decision boundary lies very close to the data samples, this behaviour is generally translated into classifiers with small margins along some discriminative directions, and large margins along the others. This property gives a constructive procedure to identify the discriminative directions exploited by a neural network (small margin directions) while it sheds new light into the inductive bias of the training dynamics of neural networks.

### 4.1. Evidence on synthetic data

We want to show that neural networks only construct boundaries along discriminative features, and that they are invariant in every other direction<sup>3</sup>. To this end, we generate a balanced training set  $\mathcal{T}_1(\epsilon, \sigma, N)$  by independently sampling  $N$  points  $\mathbf{x}^{(i)} = \mathbf{U}(\mathbf{x}_1^{(i)} \oplus \mathbf{x}_2^{(i)})$  such that  $\mathbf{x}_1^{(i)} = \epsilon y^{(i)}$  and  $\mathbf{x}_2^{(i)} \sim \mathcal{N}(0, \sigma^2 \mathbf{I}_{D-1})$ , where  $\oplus$  denotes the concatenation operator and  $\epsilon > 0$  the feature size, and  $D = 100$ . The labels  $y^{(i)}$  are uniformly sampled from  $\{-1, +1\}$ . The multiplication by a random orthonormal matrix  $\mathbf{U} \in \text{SO}(D)$  is performed to avoid any possible bias of the classifier towards the canonical basis. Note that this is a nearly separable dataset in which the only discriminative feature is parallel to  $\mathbf{u}_1$  (i.e., first row of  $\mathbf{U}$ ), while all other dimensions are filled with non-discriminative noise.

To evaluate our hypothesis we train a heavily overparameterized multilayer perceptron (MLP) with 10 hidden layers of 500 neurons using SGD (test: 100.0%). Table 1 shows the margin statistics on the linearly separable direction  $\mathbf{u}_1$ ; its orthogonal complement  $\operatorname{span}\{\mathbf{u}_1\}^\perp$ ; a fixed random subspace of dimension  $S$ ,  $\mathcal{S}_{\text{rand}} \subset \mathbb{R}^D$ ; and a fixed random subspace of the same dimensionality, but orthogonal to  $\mathbf{u}_1$ ,  $\mathcal{S}_{\text{orth}} \subset \operatorname{span}\{\mathbf{u}_1\}^\perp$ . From these values we can see that along the direction where the discriminative feature lies, the margin is much smaller than in any other direction. Therefore, we can see that the classification function of this network is only creating a boundary in  $\mathbf{u}_1$  with median margin  $\epsilon/2$  and is approximately invariant in  $\operatorname{span}\{\mathbf{u}_1\}^\perp$ .

Comparing the margin values for  $\mathcal{S}_{\text{orth}}$  and  $\mathcal{S}_{\text{rand}}$  we see

<sup>3</sup>This is indeed a desired property for any classification method, but note that for neural networks the existence of adversarial examples contests the idea of it being a reasonable assumption.

that, if the observation basis is not aligned with the features exploited by the network, the margin measurements might not be able to separate the small and large margin directions. Indeed, since  $\mathcal{S}_{\text{orth}}$  is orthogonal to the only discriminative direction  $\mathbf{u}_1$  we see that the margin values reported in this region are much higher than those reported in  $\mathcal{S}_{\text{rand}}$ . The reason for this is that the margin required to flip the label of a classifier in a randomly selected subspace is of the order of  $\sqrt{S/D}$  with high probability (Fawzi et al., 2017), and hence the non-trivial correlation of a random subspace with the discriminative features will always hide the differences between small and large margin directions.

Finally, the fluctuations in the values and the fact that the classifier is not completely invariant on  $\text{span}\{\mathbf{u}_1\}^\perp$  might indicate that the network has built a complex boundary. However, similar fluctuations and finite values in  $\text{span}\{\mathbf{u}_1\}^\perp$  would also be expected, even if the model was linear by construction and was perfectly separating the training data. In the Supp. material we provide a theoretical characterization of this phenomenon for a specific linear classifier trained on  $\mathcal{T}_1(\epsilon, \rho, N)$  using gradient descent.

## 4.2. Evidence on real data

In contrast to the synthetic data, where the discriminative features are known by construction, the exact description of the features presented in *real* datasets is usually not known. In order to identify these features and understand their connection to the local construction of the decision boundaries, we apply the proposed framework on standard computer vision datasets, and investigate if deep networks trained on real data also present high invariance along the non-discriminative directions of the dataset.

In our study, we train multiple networks on MNIST (Lecun et al., 1998) and CIFAR-10 (Krizhevsky, 2009), and on ImageNet (Deng et al., 2009) we use several of the pre-trained networks provided by PyTorch (Paszke et al., 2019)<sup>4</sup>. Let  $W, H, C$  denote the width, height, and number of channels of the images in those datasets, respectively. In our experiments we use the 2-dimensional discrete cosine transform (2D-DCT) (Ahmed et al., 1974) basis of size  $H \times W$  to generate the observation subspaces. In particular, let  $\mathcal{D} \in \mathbb{R}^{H \times W \times H \times W}$  denote the 2D-DCT generating tensor, such that  $\text{vec}(\mathcal{D}(i, j, :, :) \otimes \mathbf{I}_C)$  represents one basis element of the image space. We generate the subspaces by sampling  $K \times K$  blocks from the diagonal of the DCT tensor using a sliding window with step-size  $T$ :

$$\mathcal{S}_j = \text{span}\left\{ \text{vec}(\mathcal{D}(j \cdot T + k, j \cdot T + k, :, :) \otimes \mathbf{I}_C) \right. \\ \left. k = 0, \dots, K - 1 \right\}.$$

<sup>4</sup>In the main paper we provide the results for only some of these networks. The experiments on the rest of the networks yield similar findings and can be found in the Supp. material.

The sliding window on the diagonal of the DCT gives a good trade-off between visualization abilities in simple one-dimensional plots, and a diverse sampling of the spatial spectrum of natural images, with a well-defined gradient flowing from low to high frequencies<sup>5</sup>. We observe in practice that the DCT basis is also quite aligned to the features of these datasets, and hence it can give precise information about the discriminative features exploited by the networks.

The margin distribution of the evaluated test samples is presented in the top of Figure 2. For MNIST and ImageNet, the networks present a strong invariance along high frequency directions and small margin along low frequency ones. We will later show that this is related to the fact that these networks mainly exploit discriminative features in the low frequencies of these datasets. Notice, however, that for CIFAR-10 dataset the margin values are more uniformly distributed; an indication that the network is exploiting discriminative features along almost any direction defined by the DCT.

### 4.2.1. ADAPTATION TO DATA REPRESENTATION

Towards verifying that the proposed framework can capture the relation between the data features and the local construction of the decision boundaries, we must first ensure that the direction of the observed invariance (large margin) is related to the features presented in the dataset, rather than being just an effect of the network itself.

Based on our observation that the margin tends to be small in low frequency directions and large in high frequency ones, we choose to carefully tweak the representation of the data, such that the low frequencies are swapped with the high frequencies. In practice, if  $\mathbf{D}_{\text{DCT}}$  denotes the change of basis matrix that encodes the DCT transform, the new image representation  $\hat{\mathbf{x}}$  is expressed as  $\hat{\mathbf{x}} = \mathbf{D}_{\text{DCT}}^T \text{flip}(\mathbf{D}_{\text{DCT}} \mathbf{x})$ , where *flip* corresponds to one horizontal and one vertical flip of the DCT transformed image  $\mathbf{D}_{\text{DCT}} \mathbf{x}$ <sup>6</sup>. Thus, if the direction of the resulting margin is strongly related to the data features, the constructed decision boundaries should also adapt to this new data representation, and the margin along the invariant directions (high frequencies) should swap with the margin of the discriminative ones (low frequencies). Informally speaking, the margin distribution should “flip”.

We apply our framework on multiple networks trained on the “flipped” datasets, and the margin distribution is depicted at the bottom of Figure 2. For both MNIST and ImageNet, the directions of the decision boundaries indeed *follow* the new data representation – although they are not an exact mirroring of the original representation. This indicates that

<sup>5</sup>See Supp. material for a similar analysis performed on a grid sampling, including off-diagonal subspaces from the DCT tensor.

<sup>6</sup>See Supp. material for some visual examples.

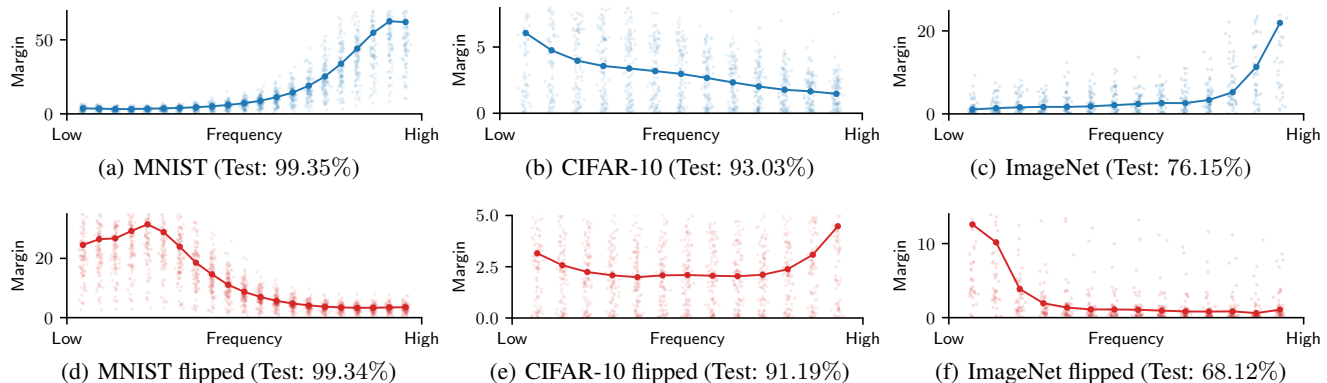


Figure 2. Margin distribution of test samples in subspaces taken from the diagonal of the DCT (low to high frequencies). The thick line indicates the median values of the margin, and the shaded points represent its distribution. **Top:** (a) MNIST (LeNet) (Lecun et al., 1998), (b) CIFAR-10 (DenseNet-121) (Huang et al., 2017) and (c) ImageNet (ResNet-50) (He et al., 2016) **Bottom:** (d) MNIST (LeNet), (e) CIFAR-10 (DenseNet-121) and (f) ImageNet (ResNet-50) trained on frequency “flipped” versions of the standard datasets.

the margin strongly depends on the data distribution, and it is not solely an effect of the network architecture. Note again that for CIFAR-10 the effect is not as obvious, due to the quite uniform distribution of the margin.

#### 4.2.2. INVARIANCE AND ELASTICITY

The second property we need to verify is that the small margins reported in Figure 2 do indeed correspond to directions containing discriminative features in the training set. In this context, we formulate the following hypothesis.

**Hypothesis 1.** For any  $z \in \mathcal{B}_{k,\ell}(f)$  there exists a unique set of discriminative directions  $\mathcal{F}_{k,\ell}(z) \subseteq \mathbb{R}^D$ . This is the smallest set spanned by a subset of all the pairwise differences between samples of class  $k$  and  $\ell$  in  $\mathcal{T}$ , such that there exists an  $\epsilon > 0$  for which all  $\mathbf{x}$  in an  $\epsilon$ -ball around  $z$  satisfy

$$\|\delta_{\mathcal{F}_{k,\ell}(z)}(\mathbf{x})\|_2 \ll \|\delta_{\mathbb{R}^D \setminus \mathcal{F}_{k,\ell}(z)}(\mathbf{x})\|_2.$$

We then say that the classifier is locally invariant to the non-discriminative directions  $\mathbb{R}^D \setminus \mathcal{F}_{k,\ell}(z)$ .

To validate this hypothesis we will use the insights of Figure 2(b) on CIFAR-10 – where, opposed to the other datasets, we assume that there are exploited discriminative features in the whole spectrum – and we will show that, by explicitly modifying its features, we can induce a high margin response in the measured curve in a set of selected directions. In particular, we create a low-pass filtered version of CIFAR-10 ( $\mathcal{T}_{LP}$ ), where we retain only the frequency components in a  $16 \times 16$  square at the top left of the diagonal of the DCT-transformed images. This way we ensure that every pairwise connection between the training images (features) has zero components outside of this frequency

subspace<sup>7</sup>.

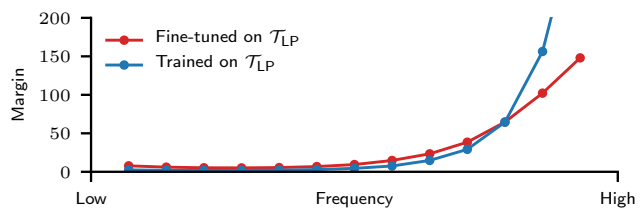


Figure 3. Median margin of test samples from CIFAR-10 for a DenseNet-121 (i) trained on CIFAR-10 and fine-tuned on  $\mathcal{T}_{LP}$  (test: 90.79%), and (ii) trained on  $\mathcal{T}_{LP}$  from scratch (test: 89.67%).

The margin distribution of CIFAR-10 test samples for a network trained on  $\mathcal{T}_{LP}$  is illustrated in Figure 3. Indeed, by eliminating the high frequency features, we have forced the network to become invariant along these directions. This clearly demonstrates that there were indeed some discriminative features in the whole spectrum of CIFAR-10, and that by effectively removing some from the training samples, the inductive bias of the learning process pushes the network to become invariant in this part of the spectrum.

Moreover, this effect can *also* be triggered during training. To show this, we start with the network studied in Figure 2(b) and continue training it for a few more epochs with a small learning rate using only  $\mathcal{T}_{LP}$ . Figure 3 shows the new median margins of this network. The fine-tuned network is again invariant on the high frequencies, thus showing the strong elasticity of the decision boundaries: Modifying the data samples (i.e., features) even during training can trigger invariance in some directions<sup>8</sup>.

Note also that when training or fine-tuning with only low

<sup>7</sup>Another example using MNIST and modifying the low fre-

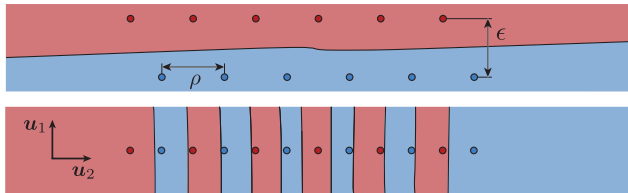


Figure 4. Cross-section of the MLP trained on  $\mathcal{T}_2(\rho = 20, \epsilon, \sigma = 1, K = 3, N = 10,000)$  with  $\epsilon = 0$  (top) and  $\epsilon = 1$  (bottom). Colors indicate regions of different classes. Axes scaled differently.

frequency features, the test accuracy of the network on CIFAR-10 only drops around 3%, which indicates that such features are enough to achieve good generalization<sup>9</sup>. This phenomenon can be explained by the invariance properties of the network. Indeed, since  $\mathcal{T}_{LP}$  has no energy in the high frequencies, the networks trained on this dataset have a tendency to uniformly extend their boundaries in this part of the spectrum, such that no high frequency perturbation can flip the classifier’s decision. However, the reverse is not true: Testing  $\mathcal{T}_{LP}$  data on a CIFAR-10 trained network only achieves 27.45% test accuracy. As the networks trained on CIFAR-10 do have boundaries in the high frequencies (c.f. Figure 2(b)), testing these networks with perturbed samples in this frequency range (i.e.,  $\mathcal{T}_{LP}$ ) can indeed greatly modify the classifier’s output.

## 5. Sensitivity to position of training samples

We finally show that the strong inductive bias of the networks towards invariance, alongside their sensitivity to the position of training samples in the input space, is responsible for the drastic increase in margin along the high frequencies when the network is adversarially trained (c.f. Figure 1). Specifically, we demonstrate that training the same architecture with a slightly perturbed version of its training samples can greatly alter the shape of the boundary. This high sensitivity to the training samples is precisely the mechanism that adversarial training exploits to produce more robust networks.

### 5.1. Evidence on synthetic data

We train multiple times an MLP with the same setup as in Section 4.1, but this time using slightly perturbed versions of the same synthetic dataset. In particular, we use a family of training sets  $\mathcal{T}_2(\rho, \epsilon, \sigma, K, N)$  consisting in  $N$  independent  $D = 100$ -dimensional samples  $\mathbf{x}^{(i)} = \mathbf{U}(\mathbf{x}_1^{(i)} \oplus \mathbf{x}_2^{(i)} \oplus \mathbf{x}_3^{(i)})$

quency features can be found in the Supp. material.

<sup>8</sup>See Supp. material for a discussion connecting this phenomenon to catastrophic forgetting (McCloskey & Cohen, 1989)

<sup>9</sup>A similar effect was shown for ImageNet on (Yin et al., 2019), although their network was only tested on the filtered data.

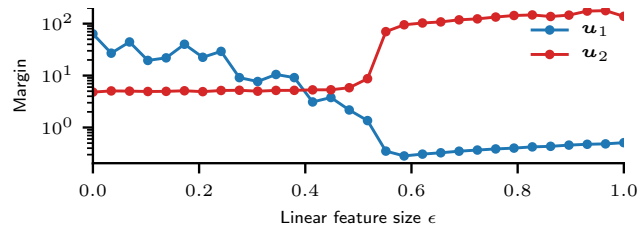


Figure 5. Median margin values along  $\mathbf{u}_1$  and  $\mathbf{u}_2$  for MLPs (test: 100% always) trained on  $\mathcal{T}_2$  for different values of  $\epsilon$  and  $\rho = 20$ .

such that  $\mathbf{x}_1^{(i)} = \epsilon y^{(i)}$ ;  $\mathbf{x}_2^{(i)} = \rho \cdot k$  when  $y^{(i)} = +1$ , and  $\mathbf{x}_2^{(i)} = \rho \cdot (k + \frac{1}{2})$  when  $y^{(i)} = -1$ , where  $k$  is sampled from a discrete uniform distribution with values  $\{-K, \dots, K - 1\}$ ; and  $\mathbf{x}_3^{(i)} \sim \mathcal{N}(0, \sigma^2 \mathbf{I}_{D-1})$  (c.f. Figure 4). Here,  $\epsilon, \rho \geq 0$  denote the feature sizes. As in Section 4.1, the multiplication by a random orthonormal matrix  $\mathbf{U} \in \text{SO}(D)$  is performed to avoid any possible bias of the network towards the canonical basis. Note that for  $\epsilon > 0$  this training set will always be linearly separable using  $\mathbf{u}_1$ , but without necessarily yielding a maximum margin classifier. Especially when  $\rho \gg \epsilon$ .

Figure 5 shows the median margin values of  $M = 1,000$  observation samples for an MLP trained on different versions of  $\mathcal{T}_2(\rho, \epsilon, \sigma, K, N)$  with a fixed  $\rho = 20$ , but a varying small  $\epsilon$ . Based on this plot, it is clear that for very small  $\epsilon$  the neural network predominantly uses the information contained in  $\mathbf{u}_2$  to separate the different classes. Indeed, for  $\epsilon < 0.2$ , the network is almost invariant in  $\mathbf{u}_1$ , and it uses a non-linear alternating pattern in  $\mathbf{u}_2$  to separate the data<sup>10</sup>. On the contrary, at  $\epsilon > 0.5$  we notice a sharp transition in which we see that the neural network suddenly changes its behaviour and starts to linearly separate the different points using only  $\mathbf{u}_1$  (c.f. Figure 4).

We conjecture that this phenomenon is rooted on the strong inductive bias of the learning algorithm to build connected decision regions whenever geometrically and topologically possible, as empirically validated in (Fawzi et al., 2018). Here, we go one step further and extend the hypothesis to the following statement.

**Hypothesis 2** (Connectedness of training samples). *The inductive bias of the learning algorithm has a tendency to build classifiers in which every pair of training samples with the same label belongs to the same decision region. If possible, connected by a straight path.*

We see Figure 5 as a validation of this hypothesis. For small values of  $\epsilon$ , it is hard for the algorithm to find solutions that connect points from the same class with a straight path, as

<sup>10</sup>Note that this particular pattern, can in principle classify any dataset with  $\rho = 20$ , no matter the value of  $\epsilon$ .

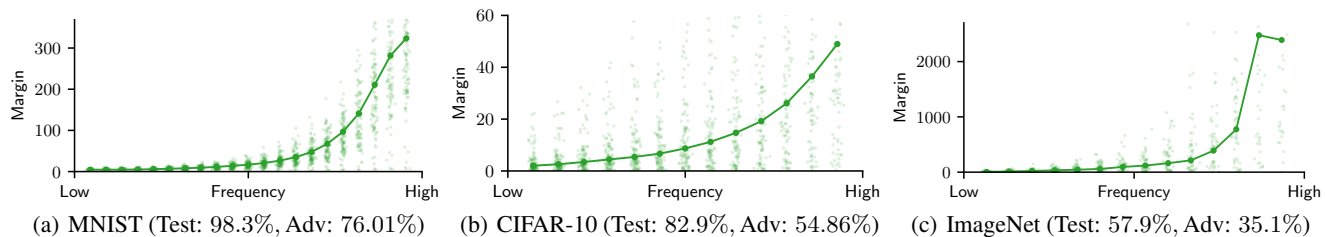


Figure 6. Margin distribution of test samples in subspaces taken from the diagonal of the DCT (low to high frequencies). Adversarially trained networks using  $\ell_2$  PGD (Madry et al., 2018) (a) MNIST (LeNet), (b) CIFAR-10 (DenseNet-121) and (c) ImageNet (ResNet-50).

this is very aligned with  $\mathbf{u}_2$ . However, there is a precise moment (i.e.,  $\epsilon = 0.5$ ) in which finding such solution becomes much easier, and that is when suddenly the algorithm starts to always converge to the linearly separated solution.

It remains unclear whether this is the only mechanism that can trigger a sharp transition in the type of learned decision boundaries, or if there are other inductive biases of the learning algorithm that can cause the same effect. In any case, we believe that the significant difference in the type of function that the algorithm learns when trained with very similar training samples (c.f. Figure 4), is an unambiguous confirmation of the sensitivity of deep learning to the exact position of its training input.

## 5.2. Connections to adversarial training

Finally, we show that one possible explanation of the success of adversarial training is that it exploits the invariance, elasticity, and sensitivity properties of the training algorithm. In this sense, Figure 6 shows the margin distribution across the DCT spectrum of a few adversarially trained networks<sup>11</sup>. As expected, the network adversarially trained on ImageNet (taken from (Engstrom et al., 2019)) is two orders of magnitude more robust (larger margin) in the high frequencies than the same network in Figure 2. Similarly, the same phenomenon is evident for the networks trained on MNIST and CIFAR-10.

Furthermore, Figure 7 shows the spectral decomposition of the adversarial perturbations crafted during adversarial training of CIFAR-10. As we can see, the energy of the perturbations remains concentrated in the low part of the spectrum during the whole training process, and has hardly any presence in the high frequencies.

Considering this, it is easy to make the analogy between the previous synthetic example and the behaviour of adversarial training on real datasets. Indeed, Figure 4 shows how slightly perturbing the training samples along a specific

<sup>11</sup>The analogous effect for the frequency-“flipped” datasets (c.f. Section 4.2.1) is illustrated in the Supp. material.

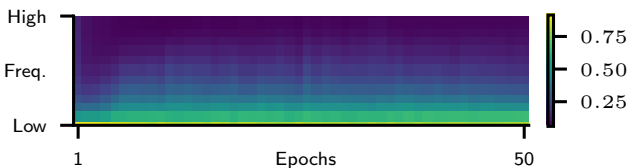


Figure 7. Energy decomposition in subspaces of the DCT (diagonal) of adversarial perturbations used during adversarial training ( $\ell_2$  PGD with  $\epsilon = 1$ ) of CIFAR-10 (DenseNet-121) on 1,000 training samples per epoch. The plot shows 95-percentile of energy.

direction  $\mathbf{u}_1$  drastically affects the margin on the orthogonal  $\mathbf{u}_2$ . Similarly, the spectral decomposition in Figure 7 demonstrates that, even if during adversarial training the training samples are mostly modified in the low frequencies, the greatest effect on margin is seen on the orthogonal high frequency directions (c.f. Figure 6).

Overall, we see how the sensitivity of the network to small changes in the training features, linked to the strong inductive bias of the algorithm towards invariance, causes an elastic response in the decision boundaries during training that can modify the discriminative and non-discriminative directions used by the classifier. This is especially clear when comparing the CIFAR-10 values in Figure 6(b) and Figure 2(b), where we evidently see that some previously used discriminative features in the high frequencies, are completely overlooked by the adversarially trained network, which, on the contrary, presents a high invariance in that part of the spectrum.

## 6. Anchor points and decision boundaries

The missing piece of Hypothesis 1 is the lack of an explicit definition of how the set of discriminative directions is constructed from the training set. Therefore, we end the paper with a conjecture on how this happens in deep learning and specifically how a few training samples can determine the complete set of discriminative and invariant directions of each segment of the decision boundary of a neural network.

**Conjecture (Anchors).** For any point  $\mathbf{z} \in \mathcal{B}_{k,\ell}(f)$  there exists a minimal set of anchor samples  $\mathcal{A}(\mathbf{z}) \subseteq \mathcal{T}$  such that

$$\exists N > 0 \text{ s.t. } \hat{F}(\mathbf{x}^{(i)}; \mathbf{z}) = y^{(i)} \quad \forall (\mathbf{x}^{(i)}, y^{(i)}) \in \mathcal{A}(\mathbf{z}),$$

where  $\hat{F}$  is a local approximation of  $F$  obtained using the  $N$ -th order Taylor expansion of  $f$  at  $\mathbf{z}$ .

The set of discriminative directions  $\mathcal{F}_{k,\ell}(\mathbf{z})$  in Hypothesis 1 is strictly generated by the pairwise differences between samples of class  $k$  and  $\ell$  in  $\mathcal{A}(\mathbf{z})$ . Besides,  $|\mathcal{A}(\mathbf{z})| \ll |\mathcal{T}|$ .

This means that modifying the position of *only* a small fraction of the training samples can induce a large change in the shape of the boundary. Note that in this conjecture the function of the anchors resembles the role that supporting vectors play in the theory of SVMs (Cortes & Vapnik, 1995), in the sense that, decision boundaries are defined by the position of some samples. However, as opposed to support vectors, anchors might not necessarily abide by the maximum margin properties that SVMs enforce. We now provide two extra pieces of evidence pointing in this direction.

**Redundancy in training samples** A central aspect of the conjecture is that there should exist many training samples that do not contribute to the creation of particular segments of the boundary. Towards this, we show that there exist datasets with redundant samples that can be removed from the training set without affecting the shape of the boundary. In particular, we show this by using an adaptation of the adversarial spheres setup (Gilmer et al., 2018; Nagarajan & Kolter, 2019), where the task is to classify data uniformly distributed on the surface of concentric  $D = 100$ -dimensional hyperspheres with different radii, such that points with radius  $r \in \{1, 3\}$  are assigned label  $y = -1$ ; and those with radius  $r \in \{4, 5\}$ ,  $y = +1$ . We train the same MLP architecture as in Section 4 using different combinations of these spheres.

Table 2 shows the test accuracy of the MLPs trained on the different hypersphere combinations, as well as an estimation of the average distance to the origin from points in the decision boundary, i.e., boundary radius. Clearly, training only with the  $r \in \{3, 4\}$  samples yields the same decision boundary as training with  $r \in \{1, 3, 4, 5\}$ , meaning that the anchors of this boundary strictly belong to the samples with  $r \in \{3, 4\}$ .

Table 2. Test accuracy and boundary radius of an MLP trained on different combinations of concentric hyperspheres.

TRAIN. $r$	RADIUS	ACC. $r \in \{1, 5\}$	ACC. $r \in \{3, 4\}$
$\{1, 3, 4, 5\}$	3.47	100.0%	99.99%
$\{1, 5\}$	2.75	100.0%	54.8%
$\{3, 4\}$	3.50	100.0%	100.0%

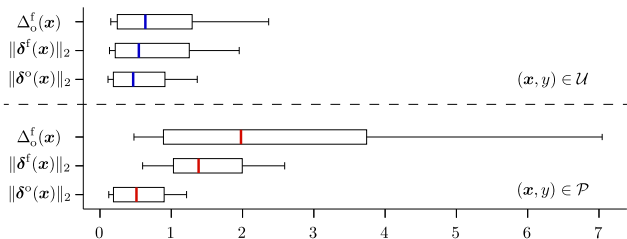


Figure 8. Margin distribution in different directions of a ResNet-18 trained on CIFAR-10 and fine-tuned on 100 DeepFool examples.

**Sensitivity to few samples** Finally, we demonstrate on real data that modifying the position of a minimal number of training samples is enough to completely change the local boundary around them. To do so, we take a ResNet-18 (test: 89%) trained on CIFAR-10, and randomly select 100 training samples  $\mathcal{P} \subset \mathcal{T}$ . We fine-tune this classifier replacing those 100 samples with  $(\mathbf{x} + \delta^o(\mathbf{x}), y)$  in  $\mathcal{P}$  (test: 90%), where  $\delta^o$  and  $\delta^f$  represent the adversarial perturbations for the original and fine-tuned network, respectively.

Figure 8 shows the magnitude of these perturbations both for the 100 adversarially perturbed points  $\mathcal{P} \subset \mathcal{T}$  and for a subset of 1,000 unmodified samples  $\mathcal{U} \subset \mathcal{T}$ . Here, we can clearly see that, after fine-tuning, the boundaries around  $\mathcal{P}$  have been completely modified, showing a large increase in the distance to the boundary in the direction of the original adversarial perturbation  $\Delta_o^f(\mathbf{x})$  for  $(\mathbf{x}, y) \in \mathcal{P}$ . Meanwhile, the boundaries around  $\mathcal{U}$  have not seen such a dramatic change. Therefore, we conjecture that  $\mathcal{P}$  do not belong to the anchor sets around the boundaries in  $\mathcal{U}$ .

Nevertheless, more evidence is required to completely prove this conjecture. We leave for future research the task of defining an efficient procedure to identify the full set  $\mathcal{A}(\mathbf{z})$  for a given  $\mathbf{z}$  in the decision boundary of a neural network.

## 7. Conclusions

In this paper, we proposed a new framework that permits to relate the features of the dataset with the margin of several samples along specific directions. In this sense, we explained how the inductive bias of the learning algorithm shapes the decision boundaries of neural networks by creating boundaries that are invariant to non-discriminative directions. We further showed that these boundaries are very sensitive to the exact position of the training samples, and that this enables adversarial training to build more robust classifiers. We believe that this new perspective can be generally used to reveal the effect of specific dataset features on the macroscopic properties of deep models and serve as a tool to obtain new insights on the intriguing properties of deep learning.

## Acknowledgements

We thank Alhussein Fawzi, Maksym Andriushchenko, and Evangelos Alexiou for their fruitful discussions and feedbacks. This work has been partly supported by the CHIST-ERA program under Swiss NSF Grant 20CH21\_180444, and partially by Google via a GCP Research Credit Award.

## References

- Ahmed, N., Natarajan, T., and Rao, K. R. Discrete Cosine Transform. *IEEE Transactions on Computers*, C-23(1): 90–93, 1974.
- Belkin, M., Hsu, D., Ma, S., and Mandal, S. Reconciling modern machine-learning practice and the classical bias–variance trade-off. *Proceedings of the National Academy of Sciences*, 116(32):15849–15854, 2019.
- Boyle, J. P. and Dykstra, R. L. A method for finding projections onto the intersection of convex sets in hilbert spaces. In *Advances in Order Restricted Statistical Inference*, pp. 28–47, New York, NY, 1986. Springer New York.
- Cortes, C. and Vapnik, V. Support-vector networks. *Machine Learning*, 20(3):273–297, 1995.
- Deng, J., Dong, W., Socher, R., Li, L. J., Kai, L., and Li, F. F. ImageNet: A large-scale hierarchical image database. In *IEEE Conference on Computer Vision and Pattern Recognition (CVPR 2009)*, pp. 248–255, Miami Beach, FL, 2009. IEEE.
- Elsayed, G., Krishnan, D., Mobahi, H., Regan, K., and Bengio, S. Large Margin Deep Networks for Classification. In *Advances in Neural Information Processing Systems (NeurIPS 2018)*, pp. 842–852, Montreal, Canada, 2018. Curran Associates, Inc.
- Engstrom, L., Ilyas, A., Santurkar, S., and Tsipras, D. Robustness (python library), 2019. URL <https://github.com/MadryLab/robustness>.
- Fawzi, A., Moosavi-Dezfooli, S. M., and Frossard, P. Robustness of classifiers: From adversarial to random noise. In *Advances in Neural Information Processing Systems (NeurIPS 2016)*, pp. 1632–1640, Barcelona, Spain, 2016. Curran Associates, Inc.
- Fawzi, A., Moosavi-Dezfooli, S.-M., and Frossard, P. The Robustness of Deep Networks: A Geometrical Perspective. *IEEE Signal Processing Magazine*, 34(6):50–62, 2017.
- Fawzi, A., Moosavi-Dezfooli, S.-M., Frossard, P., and Soatto, S. Empirical Study of the Topology and Geometry of Deep Networks. In *IEEE Conference on Computer Vision and Pattern Recognition (CVPR 2018)*, pp. 3762–3770, Salt Lake City, UT, 2018. IEEE.
- Gilmer, J., Metz, L., Faghri, F., Schoenholz, S. S., Raghu, M., Wattenberg, M., and Goodfellow, I. Adversarial Spheres. *arXiv:1801.02774*, 2018.
- Goodfellow, I. J., Shlens, J., and Szegedy, C. Explaining and harnessing adversarial examples. In *International Conference on Learning Representations (ICLR 2015)*, San Diego, CA, 2015.
- Gunasekar, S., Lee, J., Soudry, D., and Srebro, N. Characterizing Implicit Bias in Terms of Optimization Geometry. In *Proceedings of the 35th International Conference on Machine Learning (ICML 2018)*, pp. 1832–1841, Stockholm, Sweden, 2018. PMLR.
- He, K., Zhang, X., Ren, S., and Sun, J. Deep residual learning for image recognition. In *IEEE Conference on Computer Vision and Pattern Recognition (CVPR 2016)*, pp. 770–778, Las Vegas, NV, 2016. IEEE.
- He, W., Li, B., and Song, D. Decision Boundary Analysis of Adversarial Examples. In *International Conference on Learning Representations (ICLR 2018)*, Vancouver, Canada, 2018.
- Huang, G., Liu, Z., Van Der Maaten, L., and Weinberger, K. Q. Densely connected convolutional networks. In *IEEE Conference on Computer Vision and Pattern Recognition (CVPR 2017)*, pp. 2261–2269, Honolulu, HI, 2017. IEEE.
- Ilyas, A., Santurkar, S., Tsipras, D., Engstrom, L., Tran, B., and Madry, A. Adversarial Examples Are Not Bugs, They Are Features. In *Advances in Neural Information Processing Systems (NeurIPS 2019)*, pp. 125–136, Vancouver, Canada, 2019. Curran Associates, Inc.
- Jetley, S., Lord, N. A., and Torr, P. H. S. With Friends Like These, Who Needs Adversaries? In *Advances in Neural Information Processing Systems (NeurIPS 2018)*, pp. 10749–10759, Montreal, Canada, 2018. Curran Associates, Inc.
- Jiang, Y., Krishnan, D., Mobahi, H., and Bengio, S. Predicting the Generalization Gap in Deep Networks with Margin Distributions. In *International Conference on Learning Representations (ICLR 2019)*, New Orleans, LA, 2019.
- Krizhevsky, A. Learning Multiple Layers of Features from Tiny Images. Technical report, University of Toronto, Toronto, Canada, 2009.
- Lecun, Y., Bottou, L., Bengio, Y., and Haffner, P. Gradient-based learning applied to document recognition. *Proceedings of the IEEE*, 86(11):2278–2324, 1998.

- Li, Y., Ding, L., and Gao, X. On the Decision Boundary of Deep Neural Networks. *arXiv:1808.05385*, August 2018.
- Madry, A., Makelov, A., Schmidt, L., Tsipras, D., and Vladu, A. Towards Deep Learning Models Resistant to Adversarial Attacks. In *International Conference on Learning Representations (ICLR 2018)*, Vancouver, Canada, 2018.
- McCloskey, M. and Cohen, N. J. Catastrophic Interference in Connectionist Networks: The Sequential Learning Problem. *Psychology of Learning and Motivation*, 24: 109–165, 1989.
- Moosavi-Dezfooli, S.-M., Fawzi, A., and Frossard, P. DeepFool: A Simple and Accurate Method to Fool Deep Neural Networks. In *IEEE Conference on Computer Vision and Pattern Recognition (CVPR 2016)*, pp. 2574–2582, Las Vegas, NV, 2016. IEEE.
- Moosavi-Dezfooli, S.-M., Fawzi, A., Uesato, J., and Frossard, P. Robustness via Curvature Regularization, and Vice Versa. In *IEEE Conference on Computer Vision and Pattern Recognition (CVPR 2019)*, pp. 9070–9078, Long Beach, CA, 2019. IEEE.
- Nagarajan, V. and Kolter, J. Z. Uniform convergence may be unable to explain generalization in deep learning. In *Advances in Neural Information Processing Systems (NeurIPS 2019)*, pp. 11611–11622, Vancouver, Canada, 2019. Curran Associates, Inc.
- Paszke, A., Gross, S., Massa, F., Lerer, A., Bradbury, J., Chanan, G., Killeen, T., Lin, Z., Gimelshein, N., Antiga, L., Desmaison, A., Kopf, A., Yang, E., DeVito, Z., Raison, M., Tejani, A., Chilamkurthy, S., Steiner, B., Fang, L., Bai, J., and Chintala, S. PyTorch: An Imperative Style, High-Performance Deep Learning Library. In *Advances in Neural Information Processing Systems (NeurIPS 2019)*, pp. 8024–8035, Vancouver, Canada, 2019. Curran Associates, Inc.
- Ramamurthy, K. N., Varshney, K. R., and Mody, K. Topological Data Analysis of Decision Boundaries with Application to Model Selection. In *Proceedings of the 36th International Conference on Machine Learning (ICML 2019)*, pp. 5351–5360, Long Beach, CA, 2019. PMLR.
- Santurkar, S., Tsipras, D., Tran, B., Ilyas, A., Engstrom, L., and Madry, A. Image Synthesis with a Single (Robust) Classifier. In *Advances in Neural Information Processing Systems (NeurIPS 2019)*, pp. 1260–1271, Vancouver, Canada, 2019. Curran Associates, Inc.
- Sharma, Y., Ding, G. W., and Brubaker, M. A. On the Effectiveness of Low Frequency Perturbations. In *International Joint Conference on Artificial Intelligence (IJCAI 2019)*, pp. 3389–3396, Macao, China, 2019. International Joint Conferences on Artificial Intelligence Organization.
- Soudry, D., Hoffer, E., Nacson, M. S., Gunasekar, S., and Srebro, N. The Implicit Bias of Gradient Descent on Separable Data. In *International Conference on Learning Representations (ICLR 2018)*, Vancouver, Canada, 2018.
- Szegedy, C., Zaremba, W., Sutskever, I., Bruna, J., Erhan, D., Goodfellow, I. J., and Fergus, R. Intriguing properties of neural networks. In *International Conference on Learning Representations (ICLR 2014)*, Banff, Canada, 2014.
- Tsuzuku, Y. and Sato, I. On the Structural Sensitivity of Deep Convolutional Networks to the Directions of Fourier Basis Functions. In *IEEE Conference on Computer Vision and Pattern Recognition (CVPR 2019)*, pp. 51–60, Long Beach, CA, 2019. IEEE.
- Yin, D., Lopes, R. G., Shlens, J., Cubuk, E. D., and Gilmer, J. A Fourier Perspective on Model Robustness in Computer Vision. In *Advances in Neural Information Processing Systems (NeurIPS 2019)*, pp. 13255–13265, Vancouver, Canada, 2019. Curran Associates, Inc.
- Zhang, C., Bengio, S., Hardt, M., Recht, B., and Vinyals, O. Understanding deep learning requires rethinking generalization. In *International Conference on Learning Representations (ICLR 2017)*, Toulon, France, 2017.

---

## Supplementary material

---

### A. Theoretical margin distribution of a linear classifier

In this section we prove that even for linear classifiers trained on  $\mathcal{T}_1(\epsilon, \rho, N)$  the distribution of margins along non-discriminative directions will never be infinite, and that it will have a large variance (c.f. Section 4.1). This effect is due to the finiteness of the training set which boosts the influence of the non-discriminative directions in the final solution of the optimization. In particular, we show this for the linear classifier introduced in (Nagarajan & Kolter, 2019) and prove the following proposition:

**Proposition.** *Let  $f(\mathbf{x}) = \mathbf{w}^T \mathbf{x}$  be a linear classifier trained on  $\mathcal{T}_1(\epsilon, \sigma, N)$  using one-step gradient descent initialized with  $\mathbf{w} = 0$  and  $\alpha = 1$  to maximize  $f(\mathbf{x}^{(i)})y^{(i)}$  for every sample, and let  $\xi^2(\mathbf{x})$  denote the ratio between the margin in the direction of the discriminative feature  $\text{span}\{\mathbf{u}_1\}$  and the margin in an orthogonal random subspace  $\mathcal{S}_{\text{orth}} \subseteq \text{span}\{\mathbf{u}_1\}^\perp$  of dimension  $|\mathcal{S}| = S \leq D - 1$ , i.e.,*

$$\xi^2(\mathbf{x}) = \frac{\|\delta_{\mathbf{u}_1}(\mathbf{x})\|_2^2}{\|\delta_{\mathcal{S}_{\text{orth}}}(\mathbf{x})\|_2^2}.$$

*The distribution of  $\xi^2(\mathbf{x})$  is independent of  $\mathbf{x}$  and follows  $\xi^2(\mathbf{x}) \sim N\sigma^2\chi_S^2$ , where  $\chi_S^2$  denotes the Chi-squared distribution with  $S$  degrees of freedom. In particular,*

$$\text{median}(\xi^2) = \mathcal{O}\left(\frac{\sigma^2}{N\epsilon^2}S\right) \quad \text{and} \quad \text{Var}(\xi^2) = \frac{2\sigma^4}{N^2\epsilon^4}S$$

*Proof.* First, note that the weights of the classifier, after one step of GD, are

$$\mathbf{w} = \nabla_{\mathbf{w}} \sum_{i=0}^{N-1} f(\mathbf{x}^{(i)})y^{(i)} = \sum_{i=0}^{N-1} \mathbf{x}^{(i)}y^{(i)} = \mathbf{U} \sum_{i=0}^{N-1} (\mathbf{x}_1^{(i)} \oplus \mathbf{x}_2^{(i)})y^{(i)}.$$

Hence,

$$\mathbf{w} = \mathbf{U}(\mathbf{w}_1 \oplus \mathbf{w}_2) \quad \text{with} \quad \begin{cases} \mathbf{w}_1 = \sum_{i=0}^{N-1} y^{(i)}\mathbf{x}_1^{(i)} = N\epsilon \\ \mathbf{w}_2 = \sum_{i=0}^{N-1} y^{(i)}\mathbf{x}_2^{(i)} \end{cases}$$

Since  $y^{(i)}$  are uniform discrete random variables taking values from  $\{-1, +1\}$ ,  $\mathbf{x}_2^{(i)}$  are standard normal random variables independent from  $y^{(i)}$ , it can be shown that their product  $y^{(i)}\mathbf{x}_2^{(i)}$  is also a standard normal random variable. Hence,  $\mathbf{w}_2 \sim \mathcal{N}(0, N\sigma^2\mathbf{I}_{D-1})$ .

Recall that for linear classifiers the distance to the decision boundary of a point  $\mathbf{x}$  on a vector subspace  $\mathcal{S} \subseteq \mathbb{R}^D$  can be computed in closed form as

$$\|\delta_{\mathcal{S}}(\mathbf{x})\|_2 = \frac{|\mathbf{w}^T \mathbf{x}|}{\|\mathcal{P}_{\mathcal{S}}(\mathbf{w})\|_2}$$

where  $\mathcal{P}_{\mathcal{S}} : \mathbb{R}^D \rightarrow \mathbb{R}^D$  denotes the orthogonal projection operator onto the subspace  $\mathcal{S}$ . Considering this, we can compute both the margin in  $\text{span}\{\mathbf{u}_1\}$  and  $\mathcal{S}_{\text{orth}}$  as

$$\begin{aligned} \|\delta_{\text{span}\{\mathbf{u}_1\}}(\mathbf{x})\|_2 &= \frac{|\mathbf{w}^T \mathbf{x}|}{\|\mathcal{P}_{\text{span}\{\mathbf{u}_1\}}(\mathbf{w})\|_2} = \frac{|\mathbf{w}^T \mathbf{x}|}{\|\mathbf{w}_1\|_2}, \\ \|\delta_{\mathcal{S}_{\text{orth}}}(\mathbf{x})\|_2 &= \frac{|\mathbf{w}^T \mathbf{x}|}{\|\mathcal{P}_{\mathcal{S}_{\text{orth}}}(\mathbf{w})\|_2} = \frac{|\mathbf{w}^T \mathbf{x}|}{\|\mathcal{P}_{\mathcal{S}_{\text{orth}}}^{D-1}(\mathbf{w}_2)\|_2}, \end{aligned}$$

where  $\mathcal{S}_{\text{orth}}^{D-1} \subseteq \mathbb{R}^{D-1}$  is the subspace generated by the last  $D - 1$  components of the vectors in  $\mathcal{S}$ .

Squaring these distances and taking their ratio we have

$$\xi^2 = \frac{\|\delta_{\text{span}\{\mathbf{u}_1\}}(\mathbf{x})\|_2^2}{\|\delta_{\mathcal{S}_{\text{orth}}}(\mathbf{x})\|_2^2} = \frac{\|\mathcal{P}_{\mathcal{S}_{\text{orth}}^{D-1}}(\mathbf{w}_2)\|_2^2}{\|\mathbf{w}_1\|_2^2}.$$

Note now that due to the rotational symmetry of  $\mathcal{N}(0, \mathbf{I}_{D-1})$

$$\mathcal{P}_{\mathcal{S}_{\text{orth}}^{D-1}}(\mathbf{w}_2) \sim \mathcal{N}\left(0, N\sigma^2 \mathbf{U}_{\mathcal{S}_{\text{orth}}^{D-1}} \mathbf{I}_S \mathbf{U}_{\mathcal{S}_{\text{orth}}^{D-1}}^T\right),$$

where  $\mathbf{U}_{\mathcal{S}_{\text{orth}}^{D-1}} \in \mathbb{R}^{D-1 \times S}$  is a matrix whose columns form an orthonormal basis of  $\mathcal{S}_{\text{orth}}^{D-1}$ . Hence,  $\|\mathcal{P}_{\mathcal{S}_{\text{orth}}^{D-1}}(\mathbf{w}_2)\|_2^2 \sim N\sigma^2 \chi_S^2$  and

$$\xi^2 = \frac{\|\mathcal{P}_{\mathcal{S}_{\text{orth}}^{D-1}}(\mathbf{w}_2)\|_2^2}{\|\mathbf{w}_1\|_2^2} = \frac{\|\mathcal{P}_{\mathcal{S}_{\text{orth}}^{D-1}}(\mathbf{w}_2)\|_2^2}{N^2 \epsilon^2} \sim \frac{\sigma^2}{N\epsilon^2} \chi_S^2.$$

Finally, plugging in the expression for the median and variance of a Chi-squared distribution we get

$$\text{median}(\xi^2) \approx \frac{\sigma^2}{N\epsilon^2} S \left(1 - \frac{2}{9S}\right)^3,$$

and

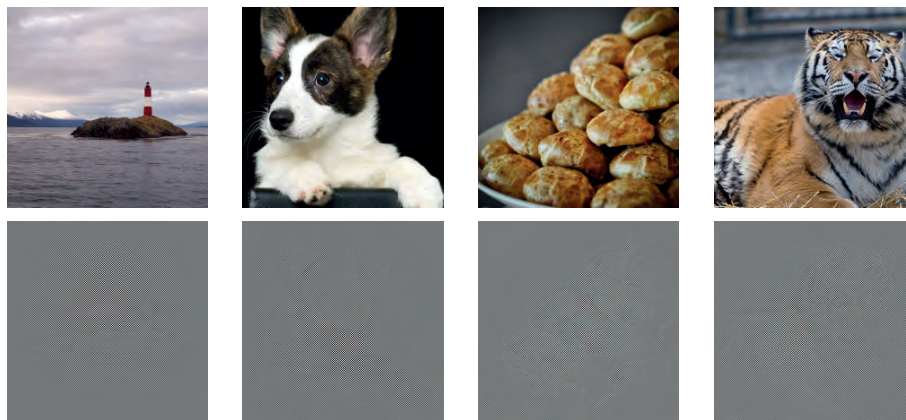
$$\text{Var}(\xi^2) = \frac{2\sigma^4}{N^2 \epsilon^4} S.$$

□

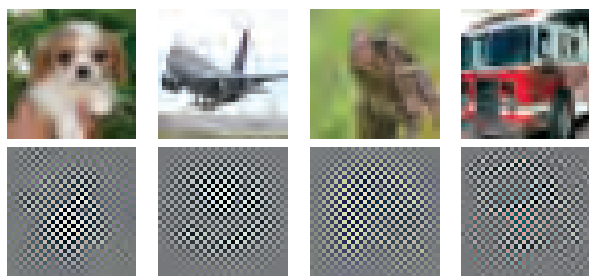
Clearly,  $\text{median}(\xi^2)$  decreases asymptotically with respect to the number of samples. Nevertheless, due to the finiteness of the training set, small but non-zero values of  $\xi^2$  are unavoidable. Similarly,  $\text{Var}(\xi^2)$  only decreases quadratically with the number of samples and grows linearly with the dimensionality of  $\mathcal{S}_{\text{orth}}$ . Hence, large fluctuations in the measured margins are expected even for linear classifiers.

## B. Examples of frequency “flipped” images

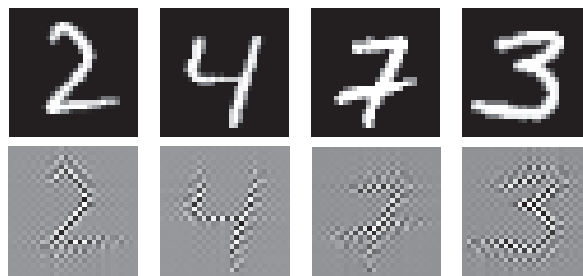
Figure 9 shows a few example images of the frequency “flipped” versions of the standard computer vision datasets.



(a) ImageNet



(b) CIFAR-10



(c) MNIST

Figure 9. “Flipped” image examples. **Top** rows show original images and **bottom** rows the “flipped” versions.

## C. Invariance and elasticity on MNIST data

We further validate our observation of Section 4.2.2 that small margin do indeed corresponds to directions containing discriminative features in the training set, but this time for a different dataset (MNIST), on a different network (ResNet-18), and using different discriminative features (high-frequency). In particular, we create a high-pass filtered version of MNIST ( $MNIST_{HP}$ ), where we completely remove the frequency components in a  $14 \times 14$  square at the top left of the diagonal of the DCT-transformed images. This way we ensure that every pairwise connection between the training images (features) has zero components outside of this frequency subspace. The margin distribution of 1,000 MNIST test samples for a ResNet-18 trained on  $MNIST_{HP}$  is illustrated in Figure 10. Indeed, similarly to the observations on CIFAR-10, by eliminating the low frequency features, we have forced an increased margin along these directions, while forcing the network to focus on the previously unused high frequency features.

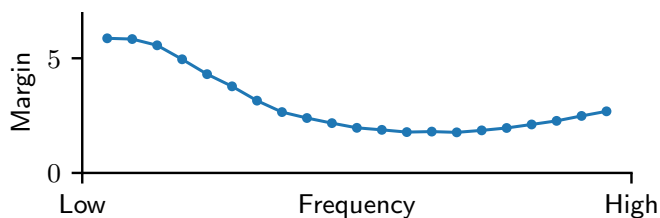


Figure 10. Median margin of test samples from MNIST for a ResNet-18 trained on  $MNIST_{HP}$  from scratch (test: 98.71%).

## D. Connections to catastrophic forgetting

The elasticity to the modification of features during training gives a new perspective to the theory of catastrophic forgetting (McCloskey & Cohen, 1989), as it confirms that the decision boundaries of a neural network can only exist for as long as the classifier is trained with the samples (features) that hold them together. In particular, we demonstrate this by adding and removing points from a dataset such that its discriminative features are modified during training, and hence artificially causing an elastic response on the network.

To this end, we train a DenseNet-121 on a new dataset  $\mathcal{T}_{LP \cup HP} = \mathcal{T}_{LP} \cup \mathcal{T}_{HP}$  formed by the union of two filtered variants of CIFAR-10:  $\mathcal{T}_{LP}$  is constructed by retaining only the frequency components in a  $16 \times 16$  square at the top-left of of the DCT-transformed CIFAR-10 images (low-pass), while for  $\mathcal{T}_{HP}$  only the frequency components in a  $16 \times 16$  square at the bottom-right of the DCT (high-pass). This classifier has a test accuracy of 86.59% and 57.29% on  $\mathcal{T}_{LP}$  and  $\mathcal{T}_{HP}$ , respectively. The median margin of 1,000  $\mathcal{T}_{LP}$  test samples along different frequencies for this classifier is shown in blue in Figure 11. As expected, the classifier has picked features across the whole spectrum with the low frequency ones probably belonging to boundaries separating samples in  $\mathcal{T}_{LP}$ , and the high frequency ones separating samples from  $\mathcal{T}_{LP}$  and  $\mathcal{T}_{HP}$ <sup>12</sup>.

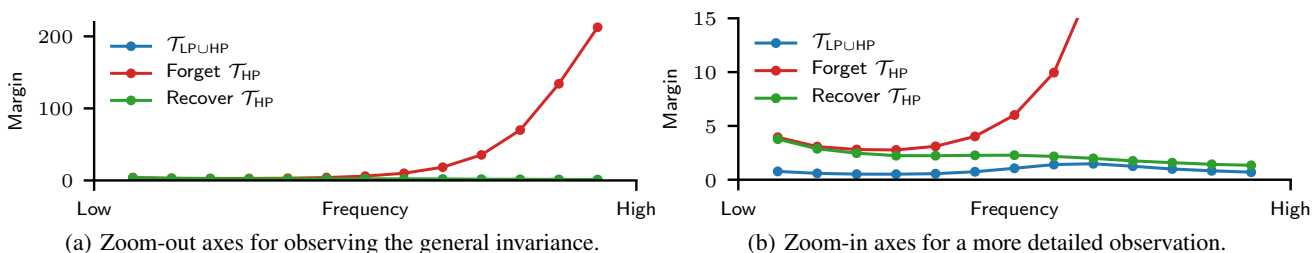


Figure 11. Median margin of  $\mathcal{T}_{LP}$  test samples for a DenseNet-121. **Blue:** trained on  $\mathcal{T}_{LP \cup HP}$ ; **Red:** after forgetting  $\mathcal{T}_{HP}$ ; **Green:** after recovering  $\mathcal{T}_{HP}$ .

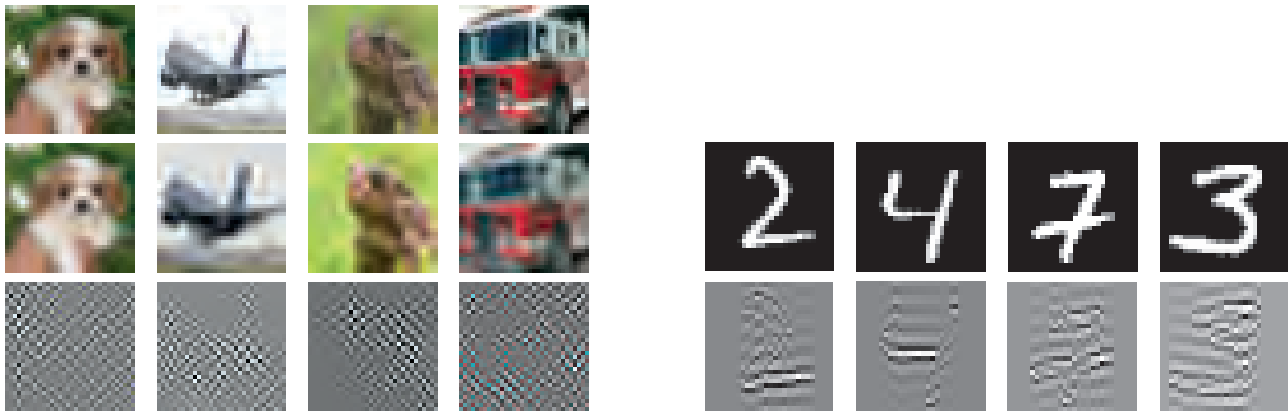
After this, we continue training the network with a linearly decaying learning rate (max.  $\alpha = 0.05$ ) for another 30 epochs, but using only  $\mathcal{T}_{LP}$ , achieving a final test accuracy of 87.81% and 10.01% on  $\mathcal{T}_{LP}$  and  $\mathcal{T}_{HP}$ , respectively. Again, Figure 11 shows in red the median margin along different frequencies on test samples from  $\mathcal{T}_{LP}$ . The new median margin is clearly invariant on the high frequencies – where  $\mathcal{T}_{LP}$  has no discriminative features – and the classifier has completely *erased* the boundaries that it previously had in these regions, regardless of the fact that those boundaries did not harm the classification accuracy on  $\mathcal{T}_{LP}$ .

Finally, we investigate if the network is able to recover the forgotten decision boundaries that were used to classify  $\mathcal{T}_{HP}$ . We continue training the network (“forgotten”  $\mathcal{T}_{HP}$ ) for another 30 epochs, but this time by using the whole  $\mathcal{T}_{LP \cup HP}$ . Now this classifier achieves a final test accuracy of 86.1% and 59.11% on  $\mathcal{T}_{LP}$  and  $\mathcal{T}_{HP}$  respectively, which are very close to the corresponding accuracies of the initial network trained from scratch on  $\mathcal{T}_{LP \cup HP}$  (recall: 86.59% and 57.29%). The new median margin for this classifier is shown in green in Figure 11. As we can see by comparing the green to the blue curve, the decision boundaries along the high-frequency directions can be recovered quite successfully.

<sup>12</sup> $\mathcal{T}_{LP}$  and  $\mathcal{T}_{HP}$  have only discriminative features in the low-frequency and high-frequency part of the spectrum, respectively.

### E. Examples of filtered images

Figure 12 shows a few example images of the filtered versions of the standard computer vision datasets used in the Section 4.2.2, C and D.



(a) CIFAR-10 (**Top** original images, **middle** low-pass and **bottom** high-pass)

(b) MNIST (**Top** original images and **bottom** high-pass)

Figure 12. Filtered image examples.

### F. Subspace sampling of the DCT

In most of our experiments with real data we measured the margin of  $M$  samples on a sequence of subspaces created using blocks from the DCT. In particular, we use a sequence of  $K \times K$  blocks sampled from the DCT tensor either from a sliding window on the diagonal with step size  $T$  or a grid with stride  $T$  (c.f. Figure 13).

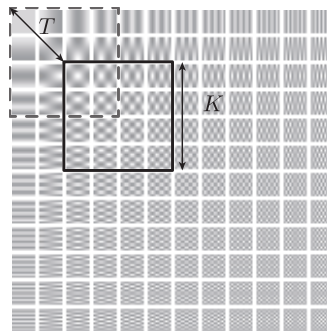


Figure 13. Diagram illustrating the main parameters defining the subspace sequence from the diagonal of the DCT.

## G. Training parameters

Table 3 shows the performance and training parameters of the different networks used in the paper. Note that the hyperparameters of these networks were not optimized in any form during this work. Instead they were selected from a set of best practices from the DAWNbench submissions that have been empirically shown to give a good trade-off in terms of convergence speed and performance. In this sense, especially for the non-standard datasets (e.g., “flipped” datasets), the final performance might not be the best reflection of the highest achievable performance of a given architecture. In fact, since the goal of our experiments is not to achieve the most robust models on such non-standard datasets, but rather investigate how the previously observed trends are represented in these new classifiers, no further hyperparameter tuning was applied.

Table 3. Performance and training parameters of multiple networks trained on different datasets. All networks have been trained using SGD with momentum 0.9 and a weight decay of  $5 \times 10^{-4}$ . For ImageNet, the training parameters are not known, since we use the pretrained models from PyTorch. For “flipped” ImageNet, the weight decay was set to  $10^{-4}$ , while for computational reasons the training was executed until the 68<sup>th</sup> epoch.

DATASET	NETWORK	TEST ACC.	EPOCHS	LR SCHEDULE	MAX. LR	BATCH SIZE
MNIST	LENET	99.35%	30	TRIANGULAR	0.21	128
	RESNET-18	99.53%				
MNIST FLIPPED	LENET	99.34%	30	TRIANGULAR	0.21	128
	RESNET-18	99.52%				
CIFAR-10	VGG-19	89.39%	50	TRIANGULAR	0.21	128
	RESNET-18	90.05%				
	DENSENET-121	93.03%				
CIFAR-10 LOW PASS	VGG-19	84.81%	50	TRIANGULAR	0.21	128
	RESNET-18	84.77%				
	DENSENET-121	93.03%				
CIFAR-10 FLIPPED	VGG-19	87.42%	50	TRIANGULAR	0.21	128
	RESNET-18	88.67%				
	DENSENET-121	88.51%				
IMAGENET	VGG-16	71.59%	–	–	–	–
	RESNET-50	76.15%				
	DENSENET-121	74.65%				
IMAGENET FLIPPED	RESNET-50	68.12%	90(68)	PIECEWISE CONSTANT	0.1	256

As mentioned in the paper, all the experiments with synthetic data were trained in the same way, namely using SGD with a linearly decaying learning rate (max lr. 0.1), no explicit regularization, and trained for 500 epochs.

## H. Cross-dataset performance

We now show the performance of different networks trained with different variants of the standard computer vision datasets and tested on the rest.

Table 4. Multiple networks trained on a specific version of MNIST, but evaluated on different variations of it. Rows denote the dataset that each network is trained on, and columns the dataset they are evaluated on. Values on the diagonal correspond to the same variation.

		MNIST	MNIST FLIPPED	MNIST HIGH PASS
MNIST	LENET	99.35%	18.73%	44.09%
	RESNET-18	99.53%	11.88%	15.73%
MNIST	LENET	10.52%	99.34%	9.87%
FLIPPED	RESNET-18	16.59%	99.52%	11.23%
MNIST	LENET	96.35%	42.36%	98.65%
HIGH PASS	RESNET-18	88.38%	21.48%	98.71%

Table 5. Multiple networks trained on a specific version of CIFAR-10, but evaluated on different variations of it. Rows denote the dataset that each network is trained on, and columns the dataset they are evaluated on. Values on the diagonal correspond to the same variation.

		CIFAR-10	CIFAR-10 FLIPPED	CIFAR-10 LOW PASS
CIFAR-10	VGG-19	89.39%	10.63%	61.4%
	RESNET-18	90.05%	10%	46.99%
	DENSENET-121	93.03%	10.3%	27.45%
CIFAR-10	VGG-19	10.77%	87.42%	10.79%
FLIPPED	RESNET-18	9.91%	88.67%	9.97%
	DENSENET-121	9.98%	88.51%	10%
CIFAR-10	VGG-19	85.16%	10.52%	84.81%
LOW PASS	RESNET-18	85.47%	10.45%	84.77%
	DENSENET-121	89.67%	10.45%	88.51%

Table 6. Multiple networks trained on a specific version of ImageNet, but evaluated on different variations of it. Rows denote the dataset that each network is trained on, and columns the dataset they are evaluated on. Values on the diagonal correspond to the same variation.

		IMAGENET	IMAGENET FLIPPED
IMAGENET	VGG-16	71.59%	0.106%
	RESNET-50	76.15%	0.292%
	DENSENET-121	74.65%	0.22%
IMAGENET FLIPPED	RESNET-50	0.184%	68.12%

## I. Margin distribution for standard networks

We show here the margin distribution on the diagonal of the DCT for different networks trained using multiple datasets using the setup specified in Section G. We also show the median margin for the same  $M$  samples on a grid from the DCT.

The first thing to notice is that, for a given dataset, the trend of the margins are quite similar regardless the network architecture. Also, regardless the evaluation (diagonal or grid), the observed margins between train and test samples are very similar, with the differences in the values being quite minimal. Furthermore, for the grid evaluations, the trend of the median margins with respect to subspaces of different frequencies (increasing from low to high frequencies) is similar to the corresponding one of the diagonal evaluations. Hence, the choice of the diagonal of the DCT is sufficient for measuring the margin along directions of the frequency spectrum. Finally, in every evaluation (diagonal or grid) and for every data set (train or test), “flipping” the representation of the data results in “flipped” margins as well, with CIFAR-10 results being an exception due to the quite uniform distribution of the margin across the whole frequency spectrum.

### I.1. MNIST

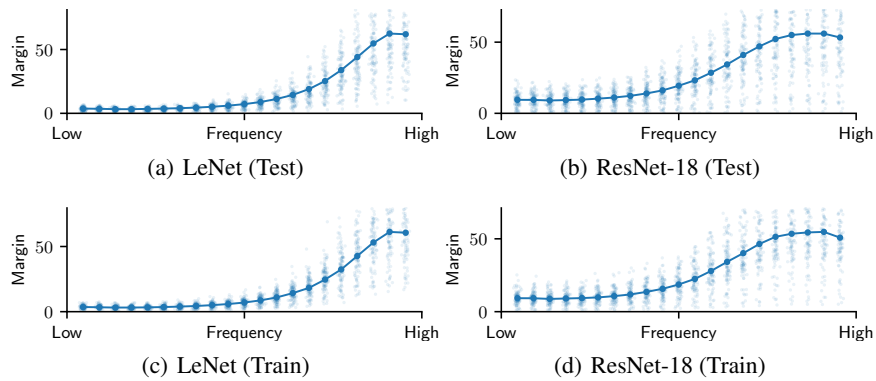


Figure 14. Diagonal MNIST ( $M = 1,000, K = 8, T = 1$ )

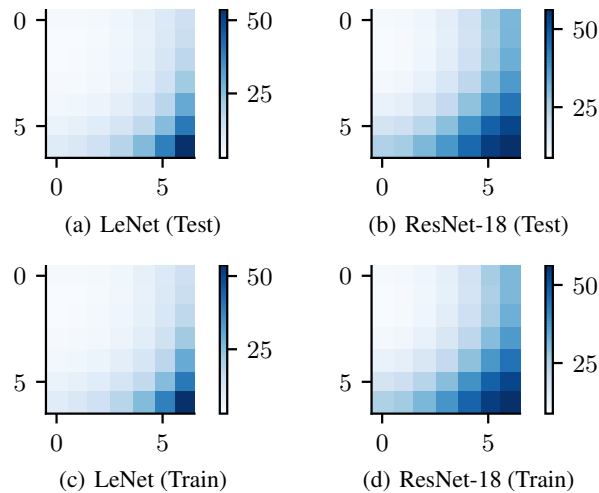


Figure 15. Grid MNIST ( $M = 500, K = 8, T = 3$ )

I.2. MNIST “flipped”

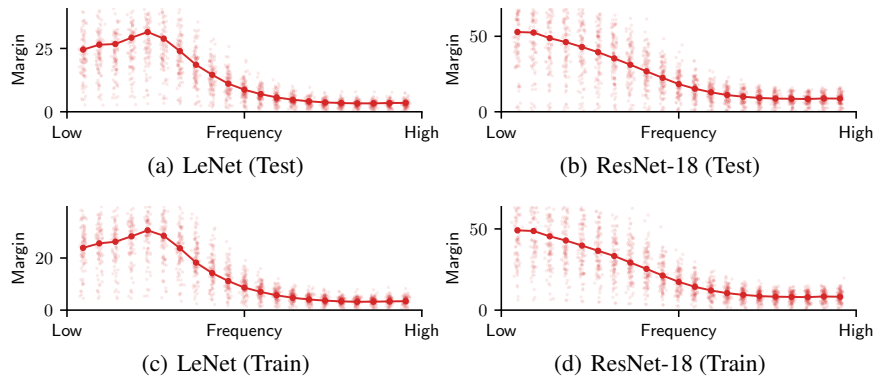


Figure 16. Diagonal MNIST “flipped” ( $M = 1,000, K = 8, T = 1$ )

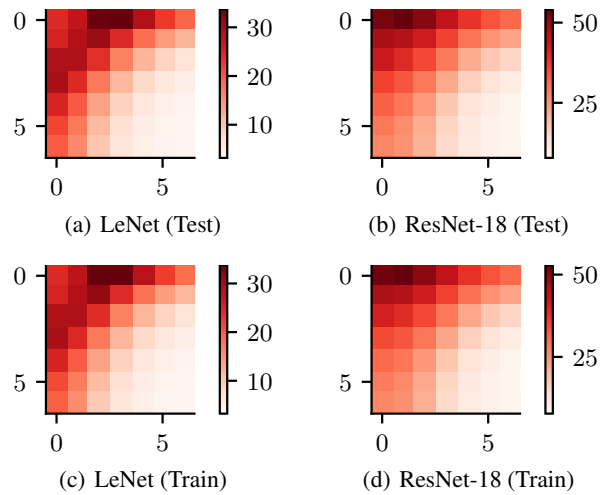


Figure 17. Grid MNIST “flipped” ( $M = 500, K = 8, T = 3$ )

I.3. CIFAR-10

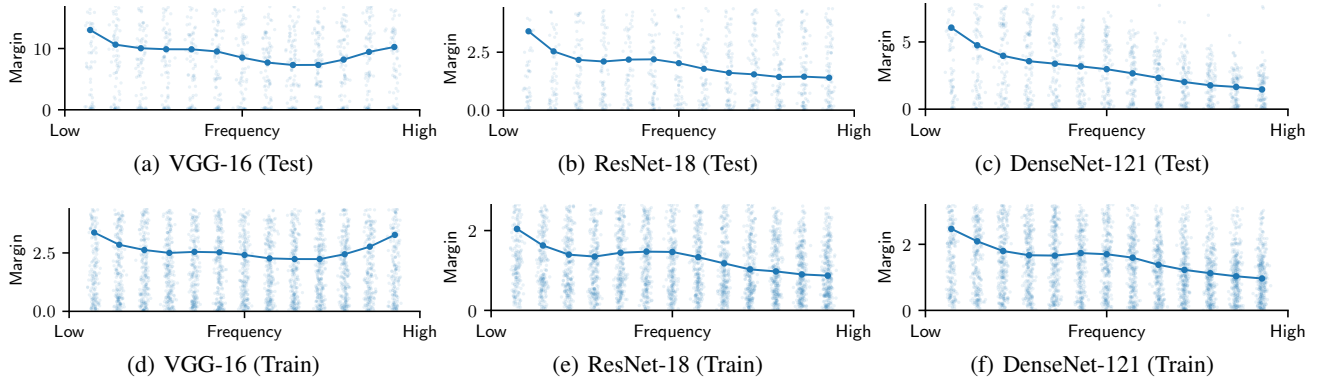


Figure 18. Diagonal **CIFAR-10** ( $M = 1,000, K = 8, T = 2$ )

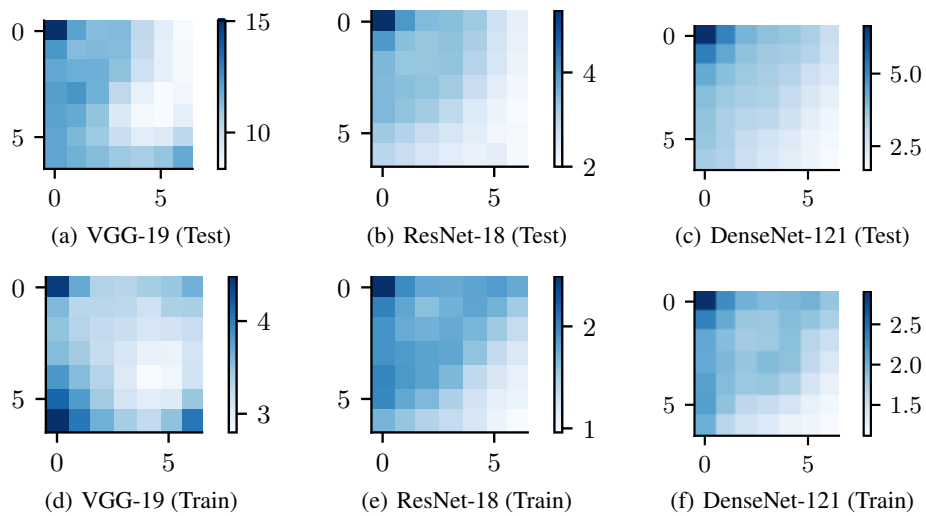


Figure 19. Grid **CIFAR-10** ( $M = 500, K = 8, T = 4$ )

I.4. CIFAR-10 “flipped”

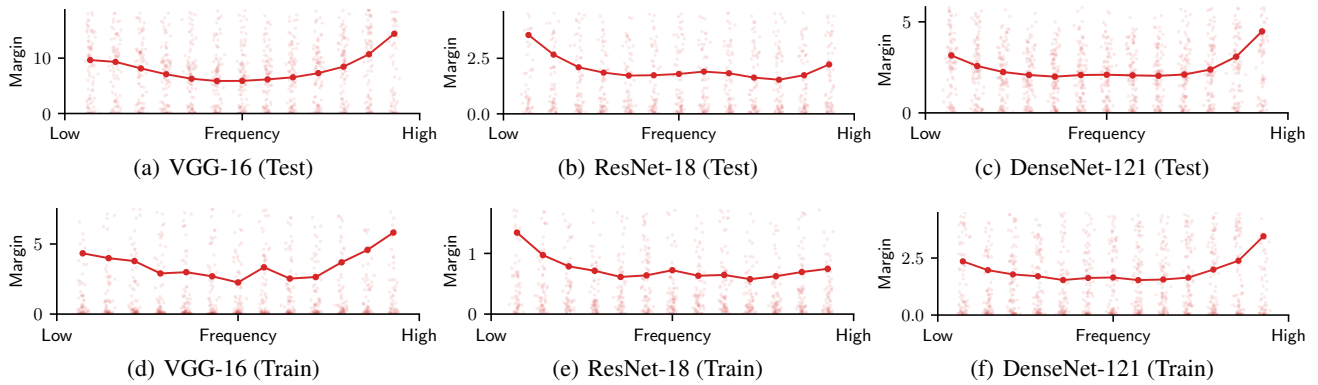


Figure 20. Diagonal **CIFAR-10 “flipped”** ( $M = 1,000, K = 8, T = 2$ )

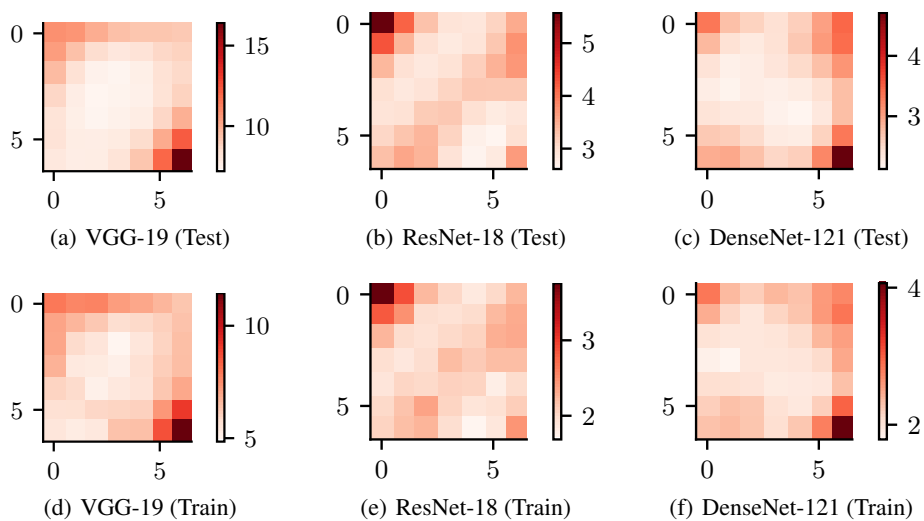


Figure 21. Grid **CIFAR-10 “flipped”** ( $M = 500, K = 8, T = 4$ )

I.5. ImageNet

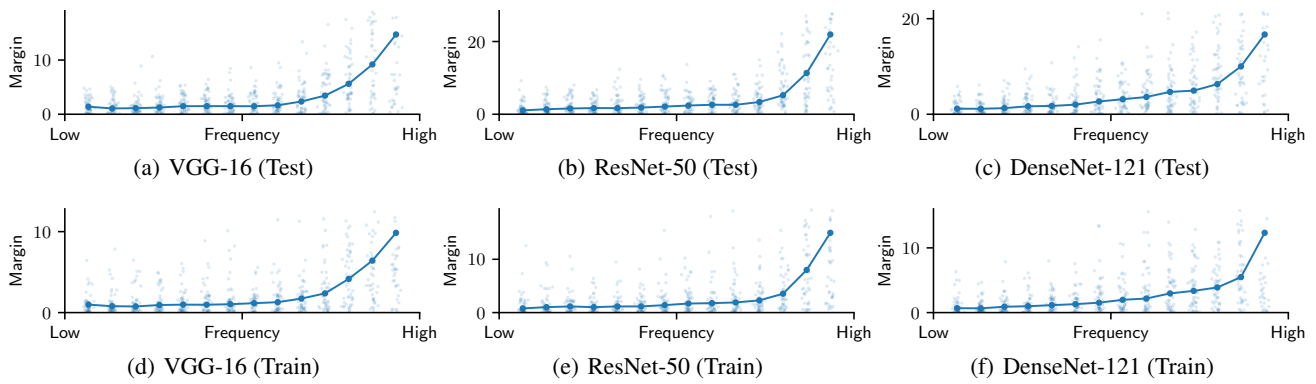


Figure 22. Diagonal ImageNet ( $M = 500, K = 16, T = 16$ )

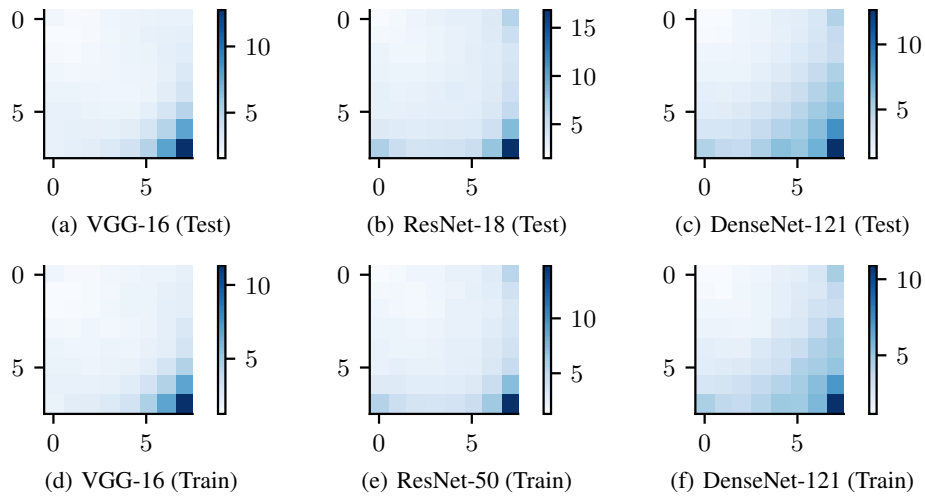


Figure 23. Grid ImageNet ( $M = 250, K = 16, T = 28$ )

## I.6. ImageNet “flipped”

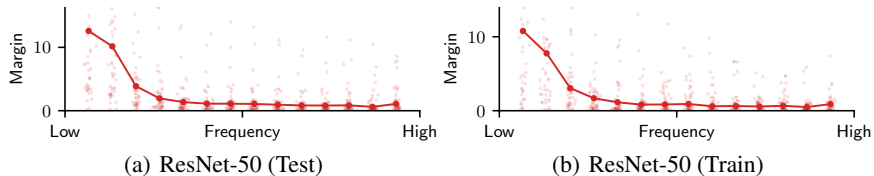


Figure 24. Diagonal **ImageNet “flipped”** ( $M = 500$ ,  $K = 16$ ,  $T = 16$ )

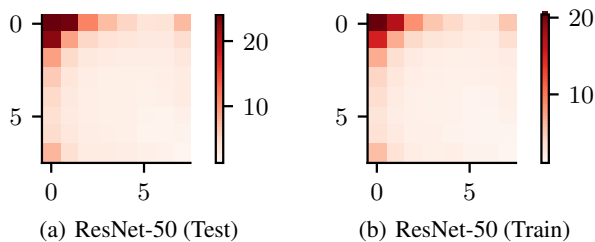


Figure 25. Grid **ImageNet “flipped”** ( $M = 250$ ,  $K = 16$ ,  $T = 28$ )

## J. Adversarial training parameters

Table 7 shows the performance and adversarial training parameters of the different networks used in the paper. Note that the hyperparameters of these networks were not optimized in any form during this work. Instead they were selected from a set of best practices from the DAWNbench submissions that have been empirically shown to give a good trade-off in terms of convergence speed and performance. Again, as stated in Section G, especially for the non-standard datasets (e.g., “flipped” datasets), the final performance might not be the best reflection of the highest achievable performance or robustness of a given architecture, since no further hyperparameter tuning was applied.

Table 7. Performance and attack parameters of multiple networks adversarially trained using  $\ell_2$ -PGD. The training parameters are similar to the ones of Table 3. For ImageNet we use the adversarially trained ResNet-50 provided by (Engstrom et al., 2019).

DATASET	NETWORK	STANDARD TEST ACC.	ADVERSARIAL TEST ACC.	EPOCHS	$\ell_2$ BALL RADIUS ( $\epsilon$ )	STEPS
MNIST	LENET	98.32%	76.01%	25	2	7
	RESNET-18	98.89%	80.26%			
MNIST FLIPPED	LENET	98.29%	74.68%	25	2	7
	RESNET-18	98.75%	81.97%			
CIFAR-10	VGG-19	73.76%	50.15%	50	1	7
	RESNET-18	82.20%	52.38%			
	DENSENET-121	82.90%	54.86%			
CIFAR-10 FLIPPED	VGG-19	71.39%	35.64%	50	1	7
	RESNET-18	73.64%	37.24%			
	DENSENET-121	78.32%	42.32%			
IMAGENET	RESNET-50	57.90%	35.16	–	3	20

## K. Description of L2-PGD attack on frequency “flipped” data

Adversarial training (Madry et al., 2018) is the de-facto method used to improve the robustness of modern deep classifiers. It consists in the approximation of the robust classification problem  $\min_f \max_{\delta \in \mathcal{C}} \mathcal{L}(f(\mathbf{x} + \delta))$  with an alternating algorithm that solves the outer maximization using a variant of stochastic gradient descent, and the inner maximization using some adversarial attack (e.g., PGD). The constraint set  $\mathcal{C} \subseteq \mathbb{R}^D$  encodes the “imperceptibility” of the perturbation.

In our case, when dealing with natural images coming from the standard datasets (i.e., MNIST, CIFAR-10 and ImageNet) we use the standard  $\ell_2$  PGD attack to approximate the inner maximization. This attack consists in the solution of  $\arg \max_{\delta \in \mathcal{C}} \mathcal{L}(f(\mathbf{x} + \delta))$  using projected steepest descent, i.e., iterating

$$\delta_{n+1} = \mathcal{P}_{\mathcal{C}} \left( \delta_n + \alpha \frac{\nabla_{\delta} \mathcal{L}(f(\mathbf{x} + \delta_n))}{\|\nabla_{\delta} \mathcal{L}(f(\mathbf{x} + \delta_n))\|_2} \right),$$

where  $\mathcal{C} = \{\delta \in \mathbb{R}^D : \|\delta\|_2 \leq \epsilon, \mathbf{0} \preceq \delta \preceq \mathbf{1}\}$ . The projection operator  $\mathcal{P}_{\mathcal{C}} : \mathbb{R}^D \rightarrow \mathbb{R}^D$  can efficiently be implemented as

$$\mathcal{P}_{\mathcal{C}}(\mathbf{x}) = \text{clip}_{[0,1]} \left( \min\{\|\delta\|_2, \epsilon\} \frac{\delta}{\|\delta\|_2} \right),$$

where

$$[\text{clip}_{[0,1]}(\mathbf{x})]_i = \begin{cases} 0 & [\mathbf{x}]_i \leq 0 \\ [\mathbf{x}]_i & [\mathbf{x}]_i < 0 \leq 1 \\ 1 & [\mathbf{x}]_i > 1 \end{cases}.$$

However, when we train using “flipped” data we need to make sure that we also transform the constraint set  $\mathcal{C}$ . Indeed, recall that the goal of training with “flipped” datasets is to check that the margin distribution approximately follows the data representation. Adversarial training tries to maximize the loss of the classifier by finding a worst-case example inside a constrained search space that is parameterized in terms of some properties of the input data (e.g., distance to a sample, or color box constraints). For this reason, if our goal is to check what happens when we only change the data representation but keep the same training scheme, it is important to make sure that adversarial training has the same search space regardless of the data representation. The flipping operator is reversible, which means we can always go back to our initial representation. Hence, by respecting the constraints over the initial representation, we make sure that the resulted adversarial examples in the new representation will still satisfy the constraints when reversed to the initial representation (image space). We achieve this reparameterization efficiently by modifying the projection operator on PGD.

Let  $\hat{\mathbf{x}} = \mathbf{D}_{\text{DCT}}^T \text{flip}(\mathbf{D}_{\text{DCT}} \mathbf{x})$  denote a frequency “flipped” data sample. The  $\ell_2$  PGD attack on this representation solves  $\arg \max_{\hat{\delta} \in \hat{\mathcal{C}}} \mathcal{L}(f(\hat{\mathbf{x}} + \hat{\delta}))$ , where  $\hat{\mathcal{C}} = \{\hat{\delta} \in \mathbb{R}^D : \mathbf{D}_{\text{DCT}}^T \text{flip}(\mathbf{D}_{\text{DCT}} \hat{\delta}) \in \mathcal{C}\}$ . Therefore, the new “flipped” PGD algorithm becomes

$$\hat{\delta}_{n+1} = \mathcal{P}_{\hat{\mathcal{C}}} \left( \hat{\delta}_n + \alpha \frac{\nabla_{\hat{\delta}} \mathcal{L}(f(\hat{\mathbf{x}} + \hat{\delta}_n))}{\|\nabla_{\hat{\delta}} \mathcal{L}(f(\hat{\mathbf{x}} + \hat{\delta}_n))\|_2} \right),$$

where  $\mathcal{P}_{\hat{\mathcal{C}}}$  can be efficiently implemented using Dykstra’s projection algorithm (Boyle & Dykstra, 1986). This is, start with  $\hat{\mathbf{x}}_0 = \hat{\mathbf{x}}, \hat{\mathbf{p}}_0 = \hat{\mathbf{q}}_0 = \mathbf{0}$  and update by

$$\begin{aligned} \hat{\mathbf{y}}_k &= \min \{ \|\hat{\mathbf{x}}_k + \hat{\mathbf{p}}_k\|_2, \epsilon \} \frac{\hat{\mathbf{x}}_k + \hat{\mathbf{p}}_k}{\|\hat{\mathbf{x}}_k + \hat{\mathbf{p}}_k\|_2} \\ \hat{\mathbf{p}}_{k+1} &= \hat{\mathbf{x}}_k + \hat{\mathbf{p}}_k - \hat{\mathbf{y}}_k \\ \mathbf{x}_{k+1} &= \text{clip}_{[0,1]} \left( \mathbf{D}_{\text{DCT}}^T \text{flip}(\mathbf{D}_{\text{DCT}}(\hat{\mathbf{y}}_k + \hat{\mathbf{q}}_k)) \right) \\ \hat{\mathbf{x}}_{k+1} &= \mathbf{D}_{\text{DCT}}^T \text{flip}(\mathbf{D}_{\text{DCT}} \mathbf{x}_{k+1}) \\ \hat{\mathbf{q}}_{k+1} &= \hat{\mathbf{y}}_k + \hat{\mathbf{q}}_k - \hat{\mathbf{x}}_{k+1}. \end{aligned}$$

The sequence  $(\hat{\mathbf{x}}_k)$  converges to  $\mathcal{P}_{\hat{\mathcal{C}}}(\hat{\mathbf{x}})$ . In our experiments we use 5 iterations of the algorithm as these are enough to achieve a small projection error.

## L. Spectral decomposition on frequency “flipped” data

Following the results presented in Section 5.2, we now show in Figure 26 the spectral decomposition of the adversarial perturbations crafted during adversarial training for the frequency “flipped” CIFAR-10 dataset on a DenseNet-121 network. In contrast to the spectral decomposition of the perturbations on CIFAR-10 (left), the energy of the frequency “flipped” CIFAR-10 perturbations (right) remains concentrated in the high part of the spectrum during the whole training process, and has hardly any presence in the low frequencies. In other words, the frequency content of the  $\ell_2$ -PGD adversarial perturbations also “flips” (c.f. Section K and M).

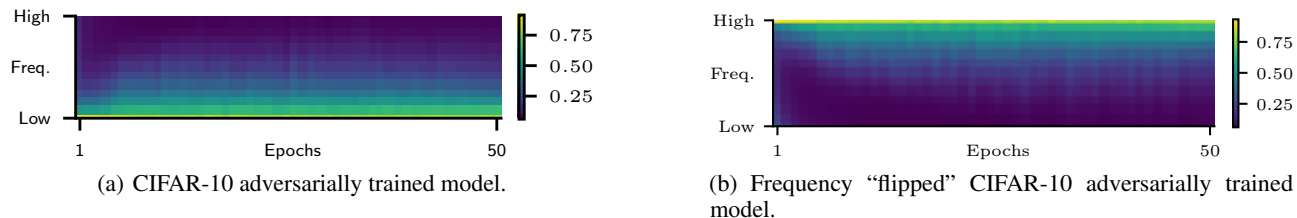


Figure 26. Energy decomposition in subspaces of the DCT diagonal of adversarial perturbations used during adversarial training ( $\ell_2$  PGD with  $\epsilon = 1$ ) on 1,000 (a) CIFAR-10 and (b) frequency “flipped” CIFAR-10 training samples per epoch for a DenseNet-121. The plot shows 95-percentile of energy.

## M. Margin distribution for adversarially trained networks

We show here the margin distribution on the diagonal of the DCT for different adversarially trained networks on multiple datasets using the setup specified in Section J. We also show the median margin for the same  $M$  samples on a grid from the DCT.

The first thing to notice for the standard datasets is that, for every network and dataset, there is a huge increase along the high-frequency directions, when compared to the margins observed in Section I. Apart from these, similarly to the observations of Section I, the margins on both train and test samples are very similar, with the differences in the values being quite minimal, while again the trend of the margins with respect to subspaces of different frequencies (increasing from low to high frequencies) is similar in both the grid and the diagonal evaluations. Finally, in every evaluation (diagonal or grid) and for every data set (train or test), “flipping” the representation of the data results in “flipped” margins as well; even for the case of CIFAR-10 where for standard training (Figure 20) the “flipping” was not obvious due to the quite uniform distribution of the margin.

### M.1. MNIST

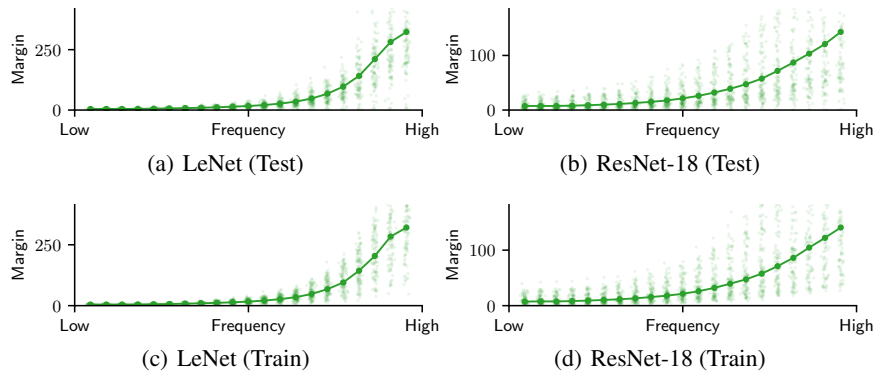


Figure 27. Diagonal MNIST adversarially trained ( $M = 1,000, K = 8, T = 1$ )

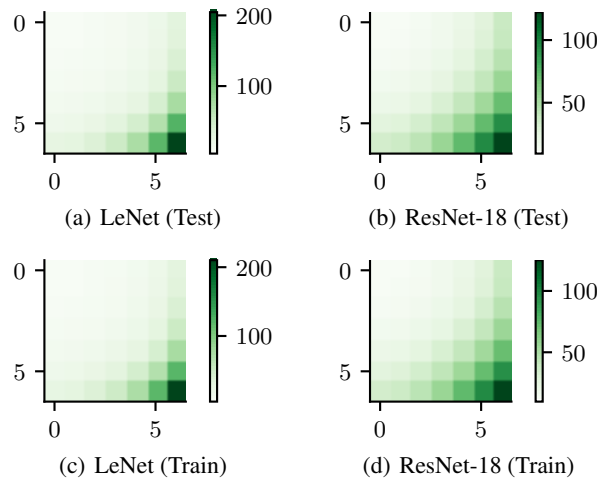


Figure 28. Grid MNIST adversarially trained ( $M = 500, K = 8, T = 3$ )

M.2. MNIST “flipped”

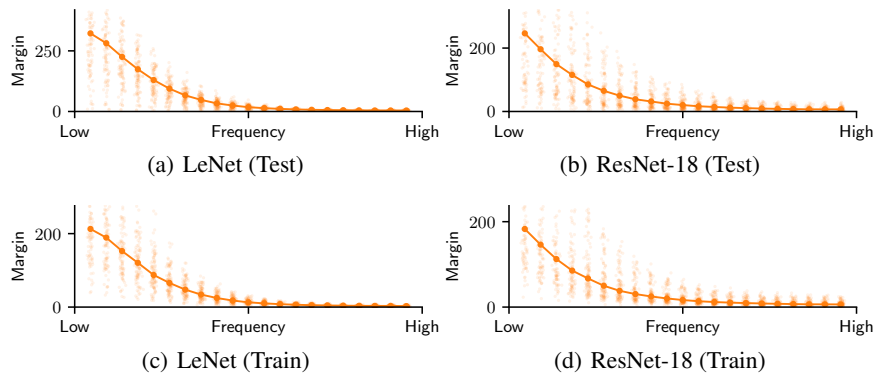


Figure 29. Diagonal MNIST “flipped” adversarially trained ( $M = 1,000$ ,  $K = 8$ ,  $T = 1$ )

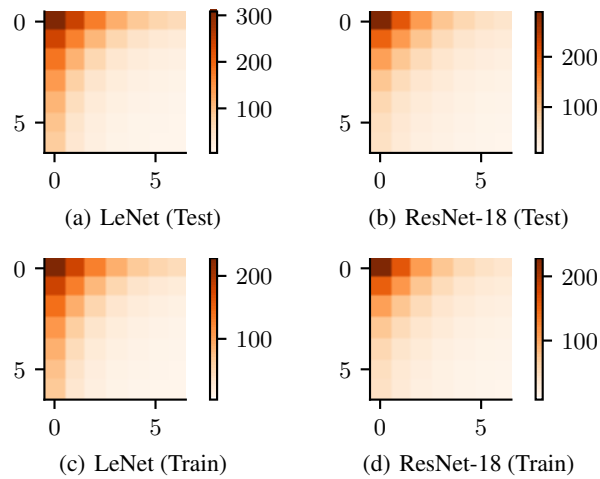


Figure 30. Grid MNIST “flipped” adversarially trained ( $M = 500$ ,  $K = 8$ ,  $T = 3$ )

M.3. CIFAR-10

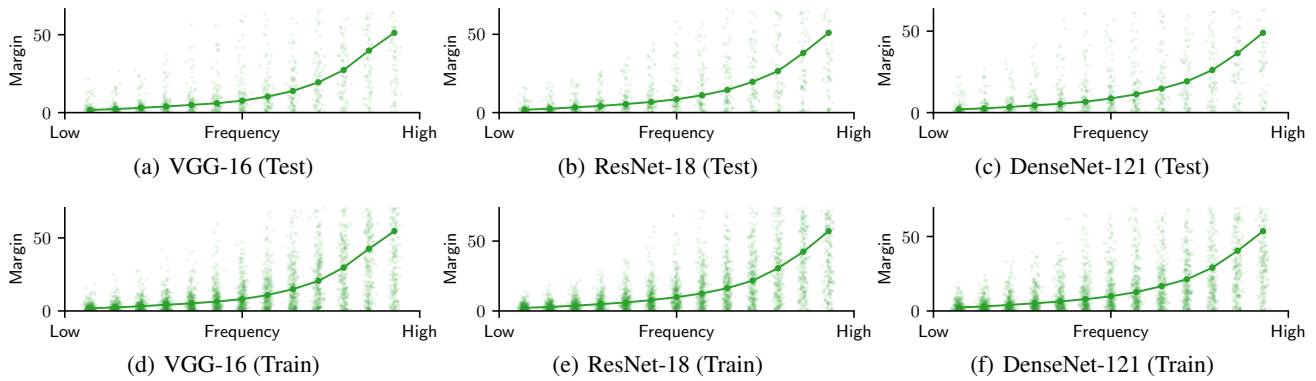


Figure 31. Diagonal **CIFAR-10** adversarially trained ( $M = 1,000, K = 8, T = 2$ )

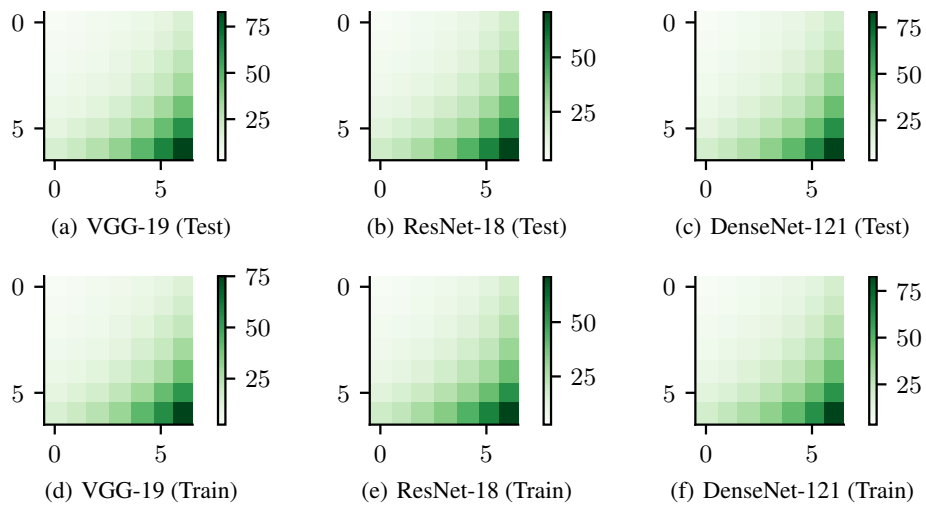


Figure 32. Grid **CIFAR-10** adversarially trained ( $M = 500, K = 8, T = 4$ )

M.4. CIFAR-10 “flipped”

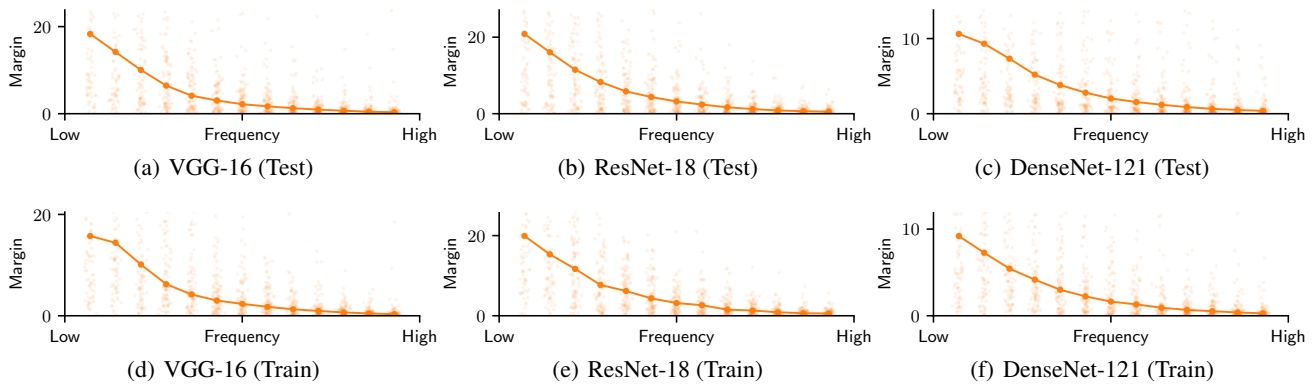


Figure 33. Diagonal CIFAR-10 “flipped” adversarially trained ( $M = 1,000, K = 8, T = 2$ )

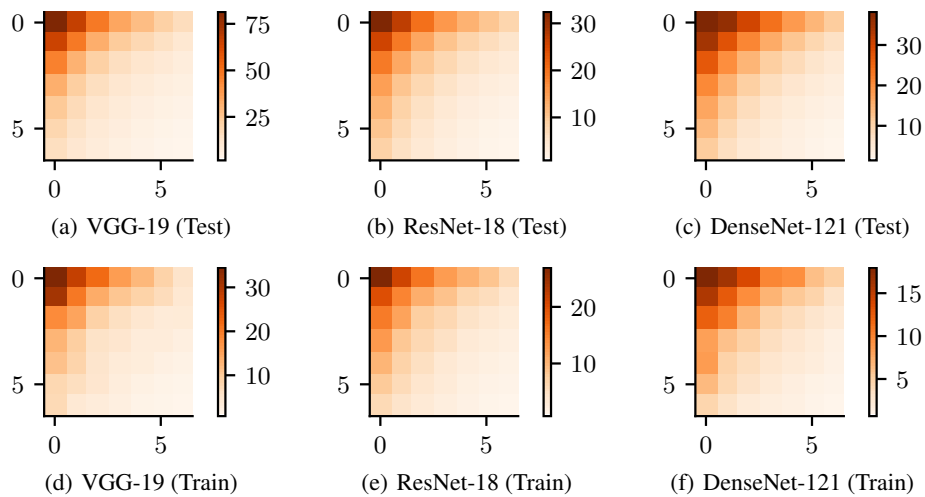


Figure 34. Grid CIFAR-10 “flipped” adversarially trained ( $M = 500, K = 8, T = 4$ )

M.5. ImageNet

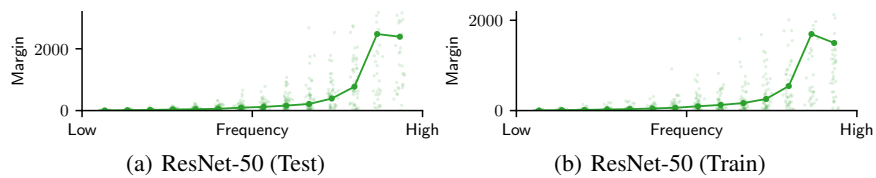


Figure 35. Diagonal ImageNet adversarially trained ( $M = 500, K = 16, T = 16$ )

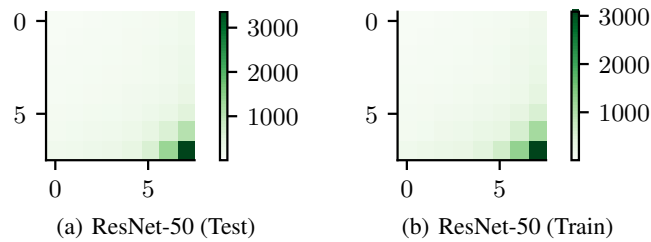


Figure 36. Grid ImageNet adversarially trained ( $M = 250, K = 16, T = 28$ )

## N. Margin distribution on random subspaces

Finally we show the same evaluation of Section I performed using a random orthonormal basis instead of the DCT basis to demonstrate that the choice of basis is indeed important to identify the discriminative and non-discriminative directions of a network. Indeed, from Figure 37 it is clear that a random basis is not valid for this task as the margin in any random subspace is of the same order with high probability (Fawzi et al., 2016).

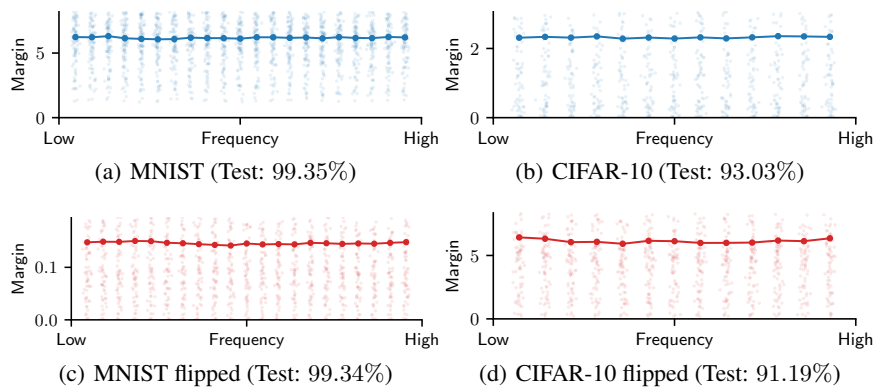


Figure 37. Margin distribution of test samples in subspaces taken from a random orthonormal matrix arranged as a tensor of the same dimensionality as the DCT tensor. Subspaces are taken from the diagonal with the same parameters as before. **Top:** (a) MNIST (LeNet), (b) CIFAR-10 (DenseNet-121) **Bottom:** (d) MNIST (LeNet) and (e) CIFAR-10 (DenseNet-121) trained on frequency “flipped” versions of the standard datasets.